공학박사 학위논문

Attenuation Profile Matching: An accurate and scan parameter-robust method for measurement of small airway dimensions in low-dose CT scans

감쇠 프로파일 정합법: 저 선량 CT 에서 촬영조건에 강인한 소기도 치수의 고정밀 측정방법

2018 년 8 월

서울대학교 융합과학기술대학원

융합과학부 방사선융합의생명전공

양 제 파

Attenuation Profile Matching:
An accurate and scan parameter-robust method for measurement of small airway dimensions in low-dose CT scans

지도 교수 김 종 효

이 논문을 공학박사 학위논문으로 제출함
2018 년 8 월

서울대학교 융합과학기술대학원
융합과학부 방사선융합의생명전공
양 제 파

양제파의 공학박사 학위논문을 인준함
2018 년 8 월

위 원 장 이 원 진 (인)

부위원장 김 종 효 (인)

위 원 임 형 준 (인)

위 원 홍 헬 렌 (인)

위 원 이 준 구 (인)

Abstract

Attenuation Profile Matching: An accurate and scan parameter robust method for measurement of small airway dimensions in low-dose CT scans

Zepa Yang

Programs in Biomedical Radiation Sciences

The Graduate School of Convergence Science and Technology

Seoul National University

The dimensions of small airways with an internal diameter of less than 2–3 mm are important biomarkers for the evaluation of pulmonary diseases, such as asthma and chronic obstructive pulmonary disease (COPD). The resolution limitations of CT systems, however, have remained a barrier to be of use for determining the small airway dimensions. A novel approach, called the attenuation profile matching (APM) method was presented, which allows for the accurate determination of the small airway dimension while being robust to varying CT scan parameters.

For generating the synthetic attenuation profiles of an airway, the point spread functions of a CT system was acquired and employed by calculating its convolution with numerical airway models with varying wall thicknesses. The dimensions of a given airway were determined as per the numerical

model yielding minimum error between the measured and the synthetic attenuation profiles across the airway.

In a phantom study with airway tubes, the APM method proved to be highly accurate in determining airway wall dimensions. The measurement error for the smallest tube (0.6 mm thickness, 3 mm diameter) was merely 0.02 mm (3.3%) in wall thickness and 0.17 mm (5.6%) in lumen diameter. In a pilot clinical test, the APM method was able to distinguish the airway wall thicknesses of COPD cases (1.16 ± 0.23 mm) from those of normal subjects (0.6 ± 0.18 mm), while the measurements using the full width at half maximum method substantially overlapped (1.45 ± 0.32 mm vs. 1.28 ± 0.30 mm, respectively) and were barely distinguishable from each other.

Our proposed APM method has the potential to overcome the resolution limitations of current CT systems and accurately determine the small airway dimensions in COPD patients.

Keywords : Attenuation Profile Matching, COPD, small airways, airway dimensions, wall thickness, point spread function

Student Number : 2013-30738

Table of Contents

List of Tables

List of Figures

1. INTRODUCTION

1.1 Background

Airway wall dimensions are important biomarkers for the evaluation of multiple pulmonary diseases, such as asthma, bronchiectasis, and chronic obstructive pulmonary disease (COPD).[1–8] The advanced imaging capabilities of Computed Tomography(CT) systems possess great potential for enabling quantitative measurements of the wall dimensions of airways accurately and non-invasively, thereby leading to better patient management during the detection, surveillance, and treatment response monitoring of airway diseases. Indeed, recent studies have stressed the importance of the ability to assess small airway wall thickening in COPD to differentiate the patient phenotype of small airway disease from that of the emphysema group, which may alter the clinical management of COPD patients.[9–11]

To date, however, CT-based measurements of small airway wall thickening have shown limited ability in terms of accuracy and reliability.[12] Studies have reported measurement errors ranging from 40% to 120% when determining airway dimensions particularly for small airways with wall thicknesses of less than 1 mm.[13] Because the major airflow resistance in COPD is known to occur at small airways,[14–17] which have an internal diameter of less than 2–3 mm,[17] improving the measurement accuracy and reliability of measurements of small airway dimensions is crucial for advancing patient phenotyping abilities and facilitating the clinical management of COPD patients.

1.2 Small airway disease

Small airway disease(SAD) is a pathologic process characterised by inflammation and fibrosis affecting small pulmonary airways. Small airway generally refers that airways have an internal diameter under 2 to 3 mm[14], usually located in the 4th or latter branch, and covers the 40% of the lung[18,19]. Disease of the small airways includes the pathological changes in the small airways of the lungs resulting from inflammation and fibrosis[20,21]. Small airways constitute the quiet zone[22,23] between the conducting and the respiratory lung zones, consisting of respiratory bronchioles, alveolar wall, and of terminal bronchioles that are devoid of cartilage and mucous secreting glands[20]. The diseases of the quiet zone[22,24,25] affect pulmonary function tests(PFT) late in the course of the disease[26]. Several studies showed that CT quantified emphysema and airway wall thickness are negatively associated with pulmonary function[27,28]. It is a distinct entity as compared to large airways disease and requires a different diagnostic screening strategy.[21]

However, it is hard to detect the dimensions of the small airway or the obstruction of the small airway in an early stage by acquiring the image from various medical imaging devices or even the usual pulmonary function tests. It is because it can be visible in tomographic images in limited resolution when a considerable amount of damage has to take place in small airways.

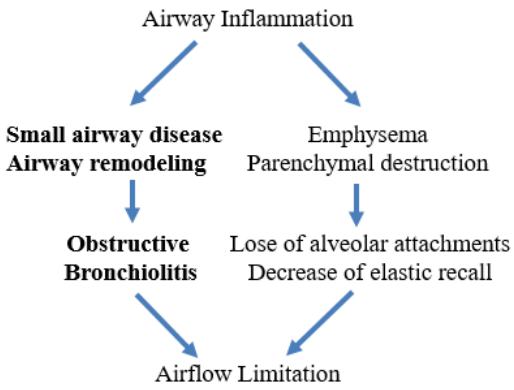

Figure 1. Flow diagram of the airway disease progress.

1.3 Problems in the current state

The correlation between wall dimensions and pulmonary function tests increase as more peripheral and smaller airways are measured.[1,29–32] However, CT scan measurements at this scale are known to overestimate wall thickness (WT) and underestimate lumen size.[33–35] Because the CT number is a weighted average of the tissue densities in an image voxel,[31] one important contributor to these errors is the partial volume effect (PVE). Typical lung CT scans provide in-plane pixel resolutions ranging from 0.6 to 0.8 mm with a slice thickness ranging 1 to 2 mm, which is comparable to the wall thickness of small airways, thereby leading to a PVE strong enough to cause measurement errors when determining the wall thickness and lumen diameter of airways.

Because these technical limitations are common and inherent to current CT imaging systems, the development of a technology that can overcome the resolution limitations and provide accurate measurements of small airway wall thickness is essential for bringing the potential of CT closer to the clinical reality of precision management for patients with airway diseases.

1.4 Previous researches

Previous studies have proposed several different approaches attempting to overcome the resolution limitations in the measurement of small airway dimensions via CT imaging.[13,14,33–39]

1.4.1 ML Solution with Gaussian PSF

Saba et al. modelled a hypothetical CT point spread function (PSF) with a Gaussian function and used an optimisation technique to yield a maximum likelihood solution for accurately measuring the inner and outer radius of the modelled airway.[13]. It was an impressive study that the model approach to the tilted airway was adopted rather than the improvement of the direct measurement method. However, the disadvantage is that the full width at half maximum (FWHM) method is inherited since the measurement method itself is the extended version of the FWHM, which is vulnerable to kernel dependency.

1.4.2 Phase congruency

R. San José Estépar et al. evaluated the phase congruency in the phase domain to accurately determine the location of the inner and outer edges of the airway wall.[33] The main purpose of the method was intensity and frequency based phase separation, which could be employed as the segmentation and thickness estimation with varying the angle of the tube. The study had well indicated the limitations of the FWHM and the intensity dependence of the reconstruction kernel and introduced the thickness estimation method using the phase information on the

frequency domain. It had such level of the robustness in noise. However, there was a limit to the fixed airway running angle.

1.4.3 Integral based method (IBM)

Weinheimer et al. employed an integral of the intensity profile across the airway wall to determine the airway wall thickness with improved accuracy.[36] This method defined the ideal physical model using the 2D integration based model within 3D centreline-based plane rotation. The need to improve the integration measurement method for the PSF is indicated, which is strongly agreed. About signal truncation, However, because of the limitation that lung tissue shows a homogeneous intensity on relatively higher dose, which leads causing harm to the patient directly or indirectly.

1.4.4 Adaptive FWHM

More recently, Wiemker et al. proposed a more straightforward approach for correcting wall thickness measurements obtained via the full width at half maximum (FWHM) method using the peak value of the intensity profile.[37] peak intensity value fallout was an essential factor that would affect selecting the half-maximum value, which occurs the result of FWHM loses its confidence. This method was a good approach, but the dependence on the kernel was not able to be ignored due to the considerable variation of the value depending on the reconstruction kernel, and there was also a problem of being vulnerable to noise.

Table 1. A partial list of previous studies and methods for measuring the airway dimensions.

Method name	Author	Key Idea	Limitation
ML Solution with Gaussian PSF	Saba et al. (Iowa Univ.)	Gaussian modelled PSF – Ellipsoid tube fitting, Maximum likelihood model	Kernel dependency
Phase congruency	Estépar et al. (Harvard Univ.)	Intensity-based thickness estimation with varying the angle of the tube	Fixed airway running angle
Integral based method (IBM)	Weinheimer et al. (Johannes Gutenberg Univ.)	Classic signal integration method with a cut-off at 10% and 90% of the signal	Image noise/slice thickness dependent
Adaptive FWHM	Wiemker et al. (Philips)	Half-maximum position variation and asynchronous lead-tail area	The same limitation with FWHM

1.4.5 Necessity for robust and accurate method

These efforts have demonstrated the feasibility of overcoming the resolution limitations of CT systems, thus allowing for accurate measurements of small airway dimensions. However, studies have also pointed out variability and biases in the measurements of the small airway dimensions depending on different reconstruction kernels and radiation dose levels,[6,13,34,39,40] which might originate from the discrepancies between the assumptions of the methods and real-world circumstances. In practice, multi-institutional studies typically include CT examinations taken with scanners from differing vendors and having different reconstruction kernels. In particular, CT examinations tend to be of lower radiation doses than in the past, and accordingly include increased image noise. These real-world circumstances might introduce sources of variation into the measurement of airway dimensions and act as a barrier to the realisation of a non-invasive and accurate method for the assessment of airway diseases via CT imaging.

Therefore, the purpose of this study was to develop a novel technique for robust and accurate measurements of small airway wall thickness and lumen

diameter. A database of PSFs obtained from modulation transfer function (MTF) measurements with varying reconstruction kernels obtained from a real-world CT scanner was created, and used them to determine the best matching airway wall dimensions, considering parenchymal lung intensity. Also, it was determined the usable part of the airway wall free from attachment to neighbouring structures and a strong partial effect due to airway orientation. It was evaluated that the accuracy and robustness of our technique using a phantom against varying reconstruction kernels and radiation doses, and present preliminary clinical results related to a small patient population with and without COPD.

2. PREREQUISITE METHODS

For emphasizing the purpose of this study, prerequisite methods with numerical simulation result were described before describing the main method. These former approaches formed the basis of proposed study. Each methods were briefly described, and their limitations were indicated.

2.1 Full width at half-maximum (FWHM)

The full width at half maximum(FWHM) is a measurement method for the length of the signal, which measures the half of the maximum value of the signal. The result of the method is the width of a half maximum amplitude measured between those points on the signal of the spectrum curve.

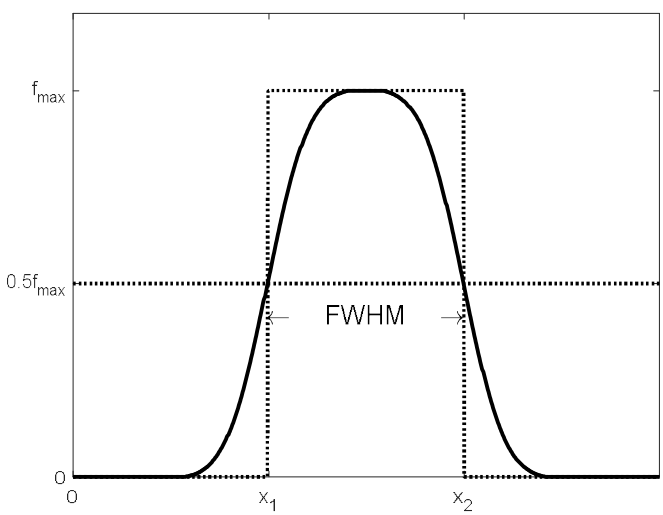

Figure 2. The graphical plot of the FWHM method.

The confidence of the FWHM method may exist when there is no distortion of the maximum intensity from the sampling rate, convolution, and so on[41]. However, the pixel spacing of the CT signal did not tend to be sufficient for full sampling the airway wall thickness range which leads the partial volume effect[42], and the maximum amplitude of the reconstruction kernel is various depending on the shape of the kernel. From these effects, the maximum intensity of the airway signal tends to be distorted[43]. In the measurement method in which half maximum intensity is the direct reference to measurement, these effects are the main problems that are failing the accurate measurements.[33,40,44]

Also, in an environment where two or more signals overlap, it is difficult to separate the boundaries between these signals since the true intensity may be spread and scattered into neighbour signal[41], which leads true peak position from ideal signal undistinguishable[43].

Figure 4 showed the numerical simulation of the signal distortion, partial volume effect.

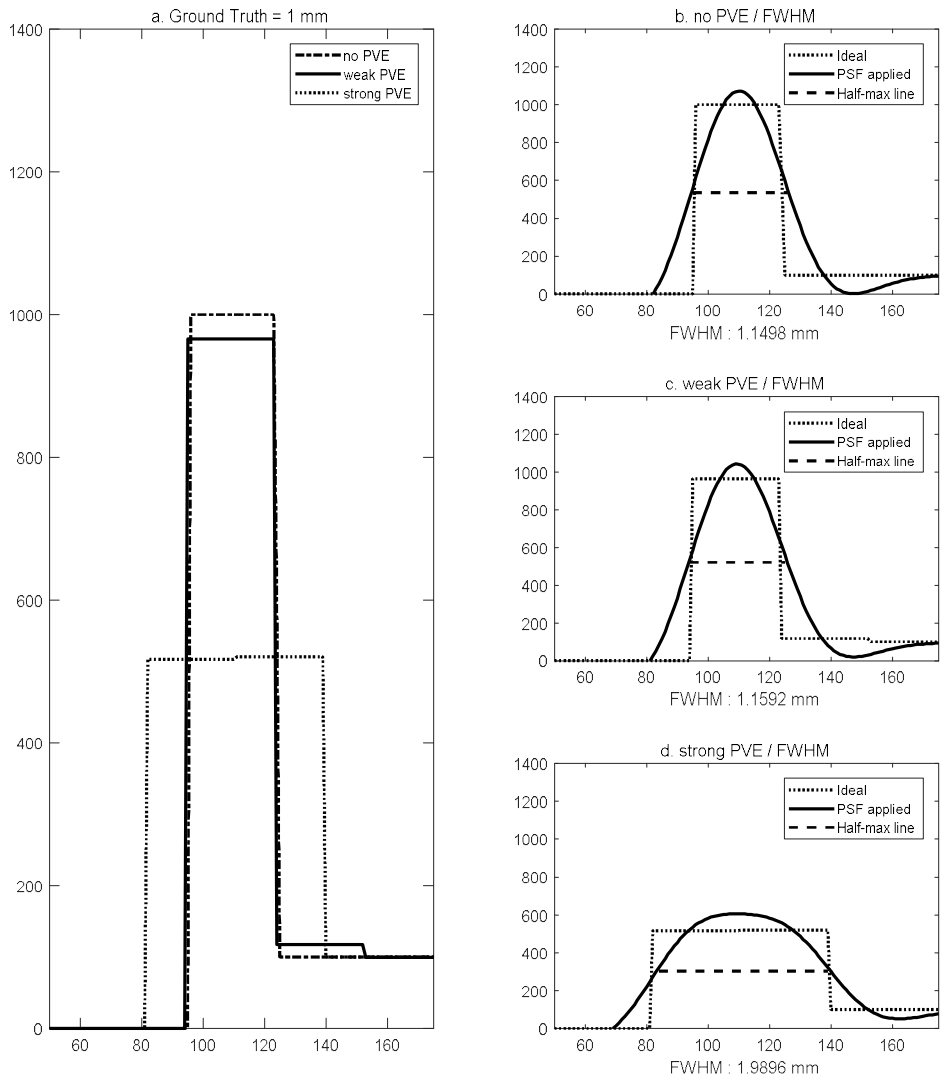

Figure 3. Partial volume effect and its FWHM-measured result in the numerical simulation.

If the length of the 'plateau' of the maximum peak is shorter than the kernel size of the PSF, peak intensity falls down[45–47]. Therefore, the 'half maximum level' length becomes broadened compared to the ideal position, which leads to an inaccurate over-estimated measurement. Furthermore, even if the length of the plateau is

sufficient, sharp reconstruction kernels must be adopted increasing the maximum intensity[48]. From this effect, the 'half maximum level' length becomes narrowed, which also leads to an inaccurate under-estimated measurement. Because it can be implied that these problems are the effects of the PSF, it is essential to calculate the exact shape and intensity of the PSF to overcome these problems. The effect and importance of the PSF/MTF for accurate measurements have been proposed in the literature[46,47,49,50]. However, it was hard to find the shape-tracking method of the PSF.

In the process of obtaining a perpendicular slice along the running angle of the centre of the airway from the axial plane image, the results would be inaccurate due to the large slice thickness, modelling, and distortion from the interpolations in multiple domains. Moreover, there is a significant dependence on the parameter for the device and environments expressed in the formula. Additionally, the precise calculation method of the variable and the training process usually affect the accuracy of the result. Due to these factors, the method has a limitation, and it could not be used efficiently in usual patient images such as screening CT scans.

A numerical demonstration was conducted to determine the effects caused by a sampling range problem. The rectangle signals with varying 0.1 to 5 mm were generated, and convoluted with PSF. Partial volume effect was simulated through the low-sampling process of idea profile. The low sampled signal was measured using the FWHM technique and compared to its ideal thickness. The pixel spacing was 0.675 mm. From the result, it was confirmed that the peak intensity could be preserved when having at least four pixels. Figure 4 showed the numerical simulation result.

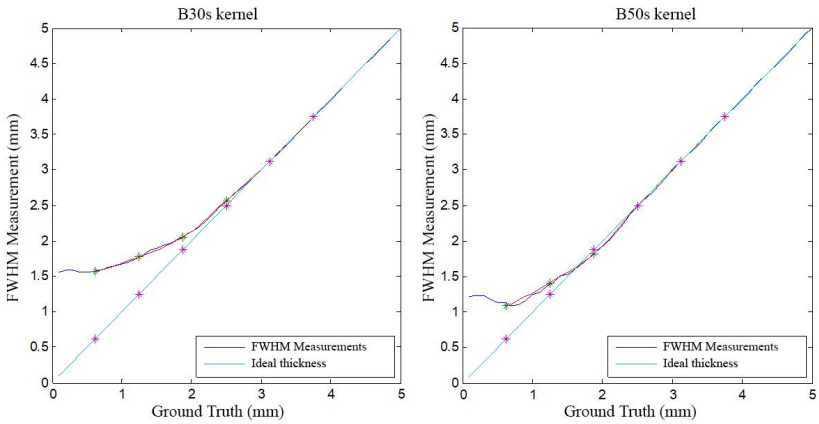

Figure 4. The result of the numerical simulation for the accuracy evaluation of FWHM measurement. Left) PSF of B30s kernel was used. Right) PSF of B50s kernel was used.

2.2 Deconvolution method

Another approach to devise a study was to focus on the fact that CT images are considered to be one signal and that they are in a convolution relationship with the signals of the actual physics[42]. Then, the ideal signal was restored by deconvolution with the obtained MTF.

Thus, the MTF was measured and took a measure of the inverse signal of the measured MTF multiplied by the frequency domain of the measured signal.

$$g(x) = f(x) * PSF\#(1)$$

$$G(\omega) = F(\omega) \times MTF\#(2)$$

$$F(\omega) = \frac{G(\omega)}{MTF}\#(3)$$

Where f was the ideal signal from the object, and g was the CT image result, and F, G were the signal in the Fourier domain of each f and g.

However, the result of MTF converges to 0 at high frequency, so that the high

frequency of the above formula converges to zero division, which derives to the infinite number. The noise of the signal was amplified by multiplying the inverse of the MTF. Therefore, this method could not be a suitable solution for images that are inherently noise-sensitive, even with using the spectral intensity-clipping filter with empirically tuned parameters.

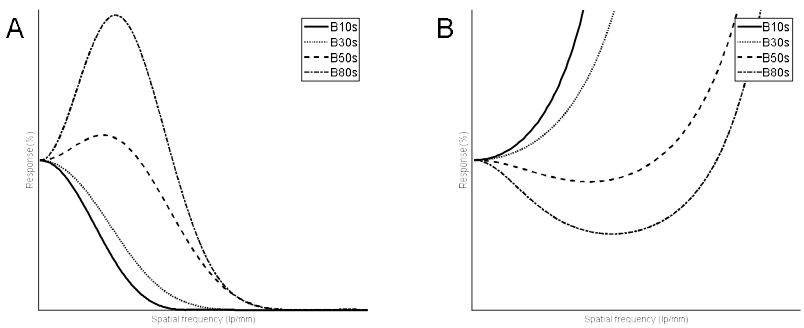

Figure 5. (A) The plot result of presampled MTF, and (B) its inverse function.

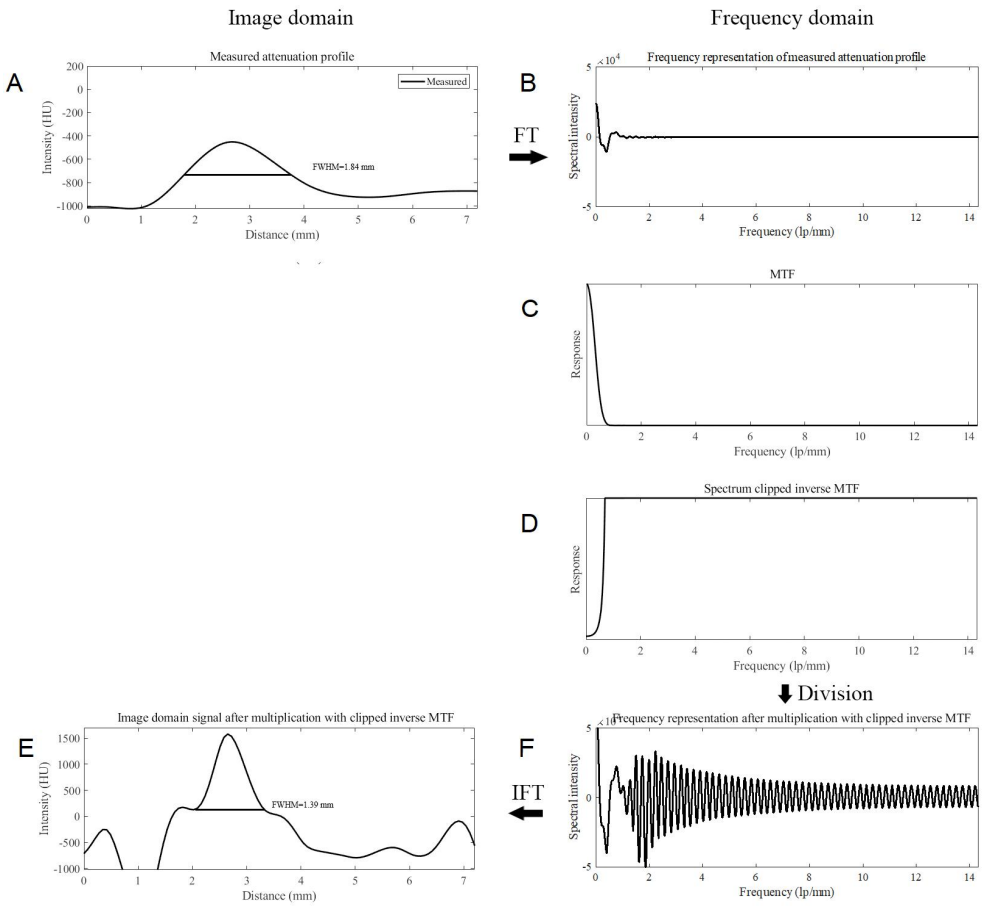

Figure 6. A) measured attenuation profile from COPDgene phantom, a tube with 0.9 mm wall thickness. Phantom was scanned at 120kVp, 200mAs with B30s kernel. B) the frequency representation of the measured attenuation profile. C) MTF kernel. D) Inverse MTF with spectrum clipping. E) signals in the image domain after the spectral intensity clipped inverse MTF multiplication. F) the frequency representation of the measured attenuation profile after the spectral intensity clipped inverse MTF multiplication.

In theoretically, the deconvolution method is a sound solution since the mathematical model may works in the ideal numerical world, without any noise

and the number of the sampling would be infinite. However, it cannot be executed in real-world problem because of the limited sampling, and the noise amplification in the high-frequency range.

Even except for these, various approaches were tried, like deconvolution in image domain rather than division in the frequency domain, empirical method to obtain the desired signal range through iterative deconvolution, level set based method, etc.

While designing the model and adopting the parameter, it is found that simulating real-alike signals through the intentional distortion of numerically generated ideal signals was not only much more straightforward than deriving an ideal signal from the calculation, but also accurate that a slight difference in numerically generated ideal signals was reflected in the signal after convolution. The proposed method was designed from this idea, with creating an ideal signature database and finding the measured signal nearest to the signal.

3. MATERIALS AND METHODS

In this section, the overall procedure of the proposed attenuation profile matching (APM) method, its evaluation step using the phantom, and patient images are described. The basic principles behind the proposed method are the modulation of the ideal attenuation profiles of the airways with the CT scan characteristics to generate a reference dataset of synthesised attenuation profiles and the use of these synthesised attenuation profiles for estimating the dimensions of the airway of interest on a CT scan. The procedure can be described in five steps, as shown in Figure 7.

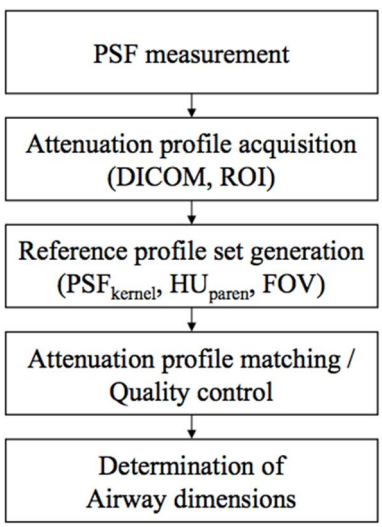

Figure 7. Schematic diagram that shows the overall procedure of the APM method.

3.1 Phantom

A commercial phantom (COPDgene Phantom, CTP674, Phantom Laboratories, Salem, NY) was used for the evaluation of the proposed APM method. The

COPDgene phantom contains six airway tubes of varying sizes (lumen diameters of 3.0 and 6.0 mm) and wall thicknesses (0.6, 0.9, 1.2, and 1.5 mm), with a background foam material causing CT attenuations similar to those of human lung parenchyma. Among the six airway tubes, four were in the perpendicular direction, and two were tilted at 30 degrees. Detailed specifications of the airway tubes are listed in Table 2. Further details of the phantom design, including the location, size, and dimensions of the air tubes, are described elsewhere.[39,51] Shown in Figure 8 are the geometric specifications and an example CT image of the phantom.

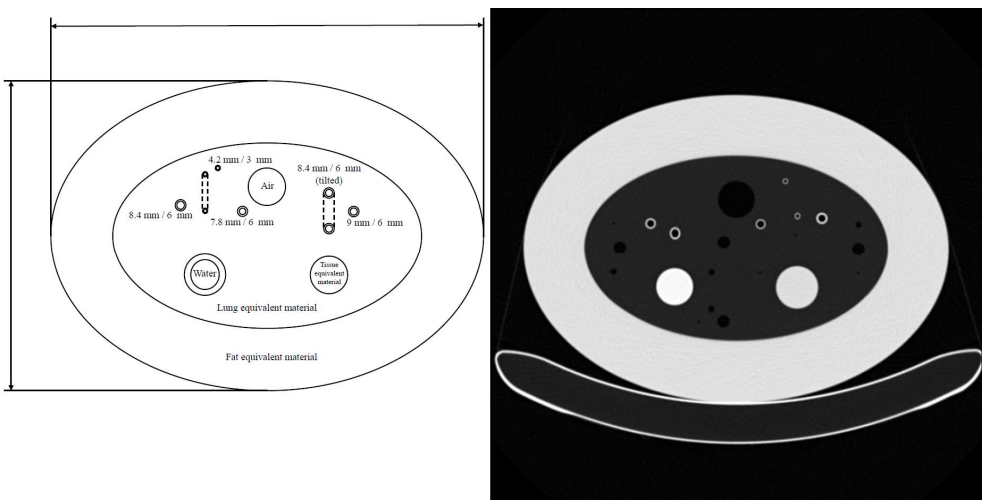

Figure 8. Geometric specifications of the COPDgene phantom and an example CT image. The image was redrawn based on the phantom design document.

Table 2. Specifications of the tubes in the phantom.

Tube No.	Outer diameter (mm)	Inner diameter (mm)	Wall Thickness (mm)	Angle (degree)	Tilt Group	Size Group
1	4.2	3	0.6	30'	Tilted	Small
2	4.2	3	0.6	0'	Non-tilted	Small
3	7.8	6	0.9	0'	Non-tilted	Medium
4	8.4	6	1.2	30'	Tilted	Medium
5	8.4	6	1.2	0'	Non-tilted	Medium
6	9	6	1.5	0'	Non-tilted	Medium

The phantom was scanned using a commercial CT scanner (Sensation 16, Siemens) and produced a set of CT images with varying scan parameters, including eight reconstruction kernels, four field-of-views (FOVs), three radiation-dose levels, and four slice thicknesses, resulting in a total of 384 CT sets. The scan conditions of our study are listed in Table 3.

Table 3. Scanning parameters and variables of the COPDgene dataset acquisition.

Recon. kernel	**Dose (mA)**	**Slice thickness**	**FOV (mm)**	**Misc.**
8 Body kernels (B10s–B80s)	25 mAs 100 mAs 200 mAs	0.75 mm, 1.5 mm, 2.25 mm, 3 mm	180 mm 250 mm 320 mm 400 mm	120 kVp 384 Combinations

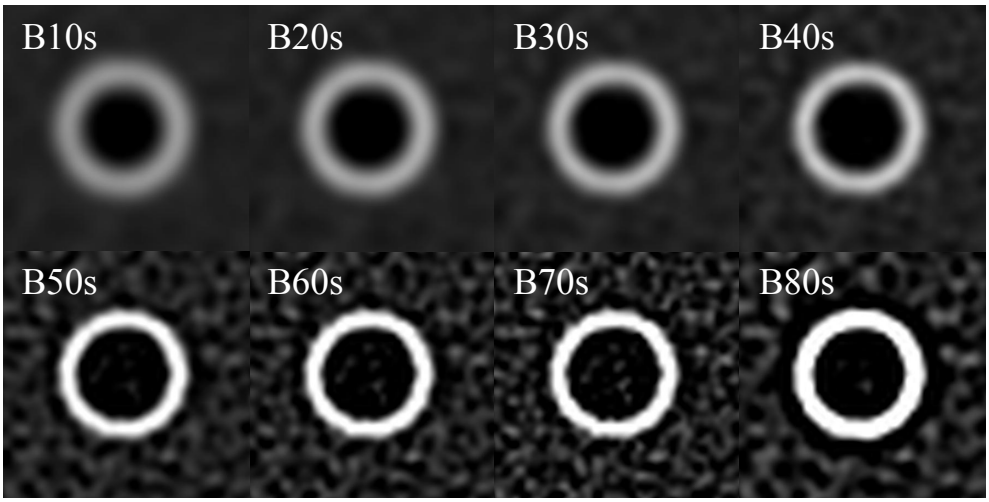

Figure 9. magnified ROI image of the tube No. 2 from the scanned COPDgene phantom. The images were reconstructed with varying reconstruction kernels, and the dependent noise and pattern was affected. The images were reconstructed with 120 kVp, 25 mAs, 0.75mm slice thickness, and 180mm FOV.

3.2 CT Point Spread Function Measurement

PSFs of the CT scanner were measured using wire-phantom scan data. A wire phantom-based MTF measurement method was used to obtain an artefact-free MTF[49,52,53], and the corresponding PSF was derived for each reconstruction kernel. A tungsten wire with a diameter size of 50 μm was scanned under 120 kVp and 200 mAs condition, followed by reconstruction with eight different kernels (B10s–B80s, Siemens) at a FOV of 180 mm.

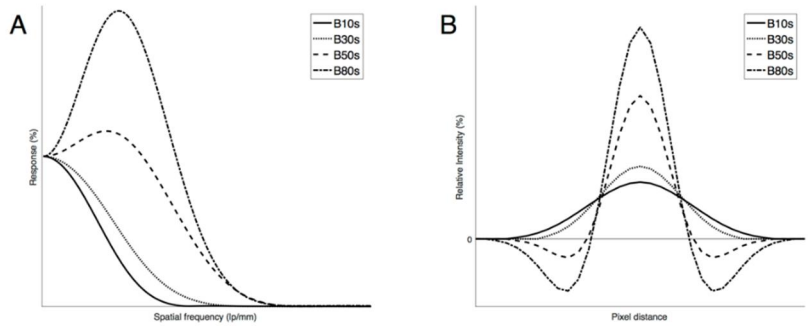

Figure 10. MTF and PSF plot result for each kernel calculated in optimal condition. A) presampled MTF measured from the method, B) derived PSF from the MTF.

For the measurement of the MTF, a tungsten wire with a diameter size of 50 μm was used. Although the wire was not assumed as the ideal point source, it may be affected to the amplitude of presampled MTF; however, since the sync function in the range of measured MTF was almost flat, which denotes the effect of the diameter of the wire can be neglected from the calculation. The frequency of the wire diameter is exceeded over the Nyquist sampling value of the standard pixel spacing range, which was nearly 0.3516 mm minimum. (FOV 180mm, 512 pixel resolution). It can be described as below formula:

$$\mathrm{MTF}_{\mathrm{measured}} = MTF_{CT} \times Wire_{50\mu m} \#(4)$$

$$\mathrm{PSF}_{\mathrm{measured}} = PSF_{CT} * Wire_{50\mu m} \#(5)$$

The wire of 50um diameter can be described as a rectangular function, which leads

$$\mathrm{PSF}_{\mathrm{measured}} = PSF_{CT} * rect(0.05) \times a \#(6)$$

a denotes Hounsfield Unit for the tungsten.

In the frequency domain, rectangle function can be calculated as a sinc function,

$$\text{rect}\left(\frac{x}{\tau}\right) = \tau\text{sinc}\left(\frac{\omega\tau}{2\pi}\right) = \tau\text{sinc}(f\tau)\#(7)$$

$$\text{MTF}_{\text{measured}} = MTF_{CT} \times 0.05 \times sinc(0.05) \times A\#(8)$$

A denotes the constant amplitude of the signal, which would be used as a normalisation.

Figure 11 showed the plot result of the numerical simulation, which denotes the relationship between the wire signal and presampled MTF.

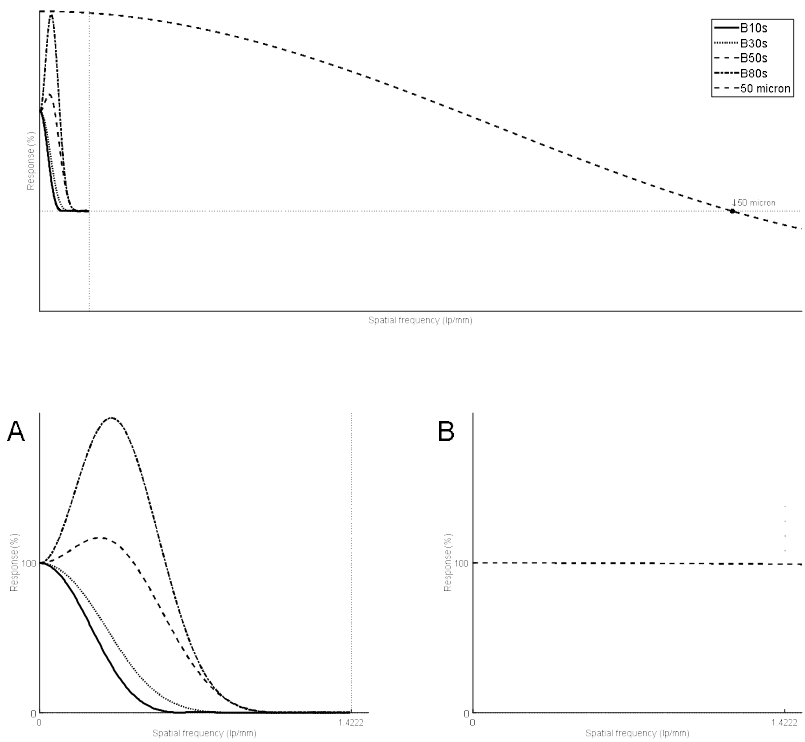

Figure 11. Upper) The response signals of MTF kernels and the sinc function of the 50 microns as plotted. Lower A) the MTF kernels in the meaningful frequency range. B) the sinc function of the 50 microns in the same range, showed the almost flat result.

3.3 Reference profile generation

A set of reference attenuation profiles of airway walls were created for determining the airway wall dimensions. First, the ideal attenuation profile I_t of an airway wall with thickness t was defined, which is the hypothetical attenuation profile of an airway wall before being translated into the CT image space (Eq. (9)). It was also defined that the measured attenuation profile g, which is the one-dimensional attenuation profile across an airway wall in Hounsfield units (HU) on a CT image. A relationship between the ideal attenuation profile I_t and the CT image space was established by performing a convolution with the PSF, and thus created the reference attenuation profile f_t (Eq. (10))

$$I_t(x) = \begin{Bmatrix} x_s \le x < x_0 : -1000 \\ x_0 \le x < x_t : HU_{tissue} \\ x_t \le x \le x_e : HU_{paren} \end{Bmatrix} \#(9)$$

$$f_t(x) = \int_{-\infty}^{\infty} I_t(\tau) h(x-\tau) d\tau \ \#(10)$$

In Eq. (10), $h(\delta - x)$ indicates the PSF of the CT system.

The ideal profile of an airway wall was modelled as a one-dimensional signal with a length of 7 mm, which consisted of three consecutive rectangular boxes, each with different lengths and attenuations. The first box represented the lumen part filled with air, and was modelled to have a length of 2 mm and −1000 HU. The second box represented the wall tissue, and was modelled to have a varying length ranging from 0.3 to 3.0 mm.

The attenuation of the wall tissue HU_{tissue} was set differently depending on the experiment type. In the phantom experiment, HU_{tissue} was determined by averaging the measured attenuation on the large rod of the phantom, which has the

same tissue-equivalent material as the airway mimicking tube. In the patient experiment, HU_{tissue} was determined by averaging the measured attenuation on CT images along the trachea wall of 15 normal patients. In our experimental setting with 120 kVp, HU_{tissue} was 150 HU in the phantom experiment and 0 to 130 HU in the patient experiment. The third box was for the lung parenchyma, which occupied the rest of the profile (5 mm – t). The parenchymal attenuation, HU_{paren}, was determined by averaging the attenuation within the segmented lung area on the CT images of interest. The segmentation of the lung was carried out using a seeded-region-growing technique by placing a seed pixel on the lung parenchyma and setting the tolerance range from −900 to −600 HU. The seed point for each lung was determined automatically by considering the size, orientation, and attenuation range of the lungs in the CT images.

To ensure the precision of the determined airway wall thickness regardless of the pixel spacing of the CT images, the sampling interval of the reference attenuation profile was set to 0.1 mm. Then, the reference attenuation profile f_t was generated by calculating the convolution of I_t with the PSF corresponding to the reconstruction kernel of a given CT image. Thus, when a CT image was taken and the $HU_{paren}$was obtained from the lung field, a total of twenty-eight I_t were created, with thicknesses t ranging from 0.3 mm to 3.0 mm at 0.1-mm interval, and then their counterpart set of f_t were generated.

Shown in Figure 12 is a graphical illustration of our reference profile generation procedure, along with comparisons of the generated reference profiles for different reconstruction kernels and varying wall thicknesses.

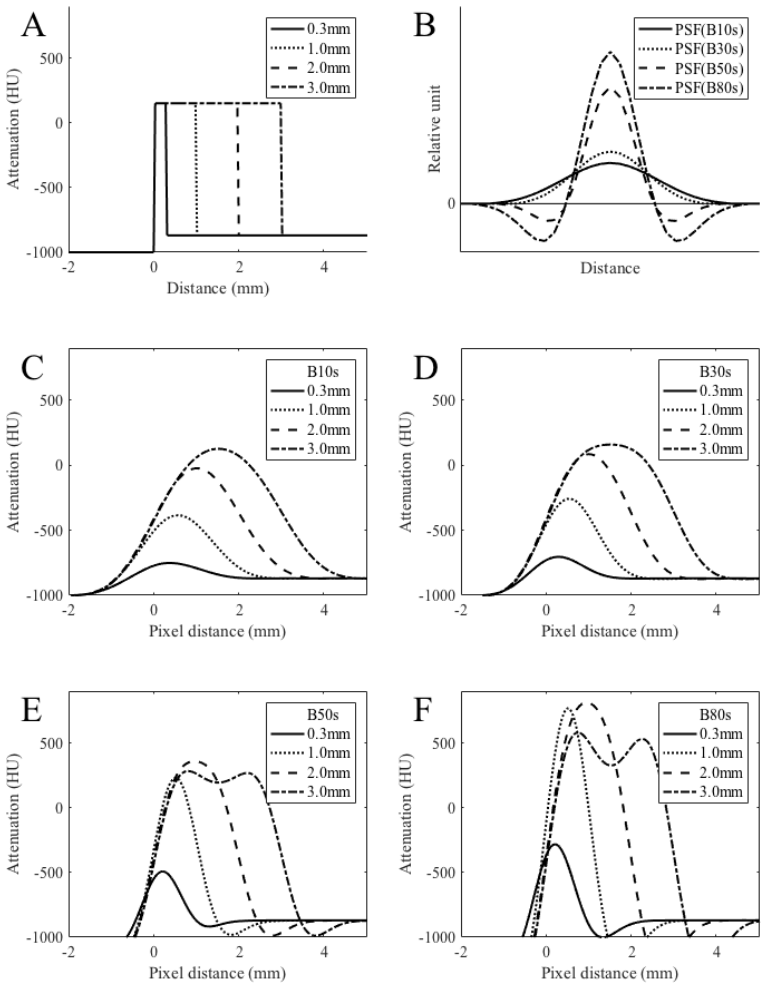

Figure 12. Graphical illustration of the reference profile generation procedure. A) Ideal attenuation profiles with wall thicknesses of 0.3–3.0 mm. B) Example PSFs of selected reconstruction kernels. Attenuation values below −1000 HU were truncated considering the intensity range limitation of the CT number. Synthesized reference profiles for (C) B10s, (D) B30s, (E) B50s, and (F) B80s kernels.

3.4 Attenuation Profile Matching

In our scheme, a seed point was chosen by the user at the centre of the region of interest (ROI) of the airway lumen, and then attenuation profiles across the

airway wall were angular sampled, centred on the seed point at 5-degree interval. Thus, 72 samples of measured attenuation profiles were obtained from the ROI of each airway lumen.

For each measured attenuation profile, the best matching reference attenuation profile was determined by comparing the similarity between the measured and the reference attenuation profile set.

A weighted distance measure was defined to assess the similarity between the measured and the reference attenuation profiles, as shown in Eq. (11). A weight function was designed to obtain higher weights on more 'informative' data points that exhibit steep changes and which potentially act as robust landmarks in distance assessment for noisy attenuation profile curves.

$$E(g,f) = \left\| \sqrt{|(w_0 + w_1 f_t'(x) + w_2 f_t''(x))(g(x - x_0) - f_t(x))|} \right\|_2 \#(11)$$

$$E_{min} = \underset{t}{arg\,min}\ \underset{x_0}{arg\,min}\, E(g,f) \#(12)$$

In these equations, g indicates the measured attenuation profile, and f_t denotes the reference attenuation profile of thickness *t*. Weight w_0 is responsible for the Euclidian distance between g and f_t, w_1 is responsible for the first derivative and was intended to yield a better alignment between g and f_t with higher emphasis on the portion of the profile at the wall transition, while w_2 is responsible for the second derivative and was intended to force the selection of the profile pair with the most similar peak shapes. Weights w_0, w_1, and w_2 were set empirically to 0.5, 0.75, and 0.25, respectively. The derivatives were calculated on the reference attenuation profile.

In comparing the two signatures, there were some important factors to be

considered. Since it was based on the PSF form, it was important to note how much the shape of the PSF was reflected in the kernel. The shape of the PSF can be derived as the curvature of the reference profile set. The current maximum intensity and index of the profiles were also a significant factor. As described in the introduction part, peak intensity tends to be fall out from various effects. Since the convolutional effect, the index of the peak intensity is usually jittered from the original centre of the ideal index, so the shift of the index is also an important factor to match two profile curves. Also, the increase/decrease ratio of the lead and trail of the curve were also a factor to be concerned, which might be affected by the overshoot/undershoot effect of the kernel. To integrate these factors into an equation, first derivatives and second derivatives were added in the conventional sum of squared-root difference (SSRD).

Figure 13 showed the result of the reference profile and its first and second derivatives regarding the defined formula Eq. (12).

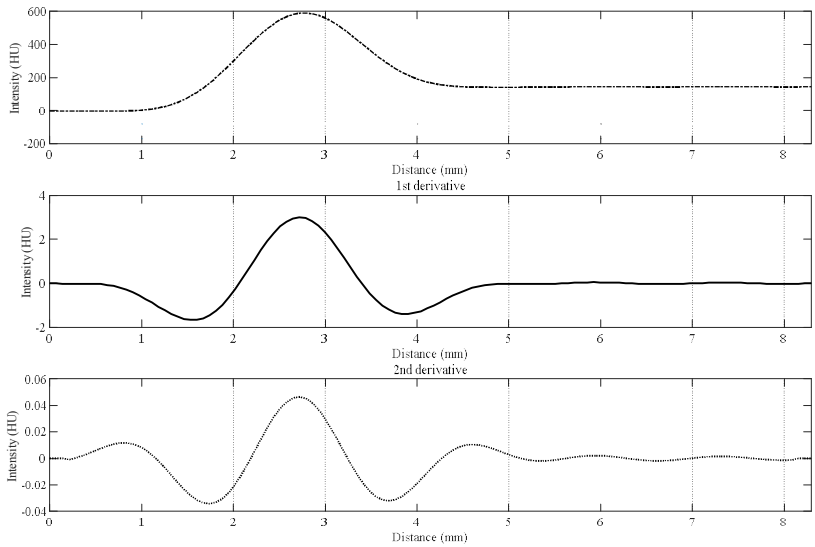

Figure 13. the plot result of the reference profile and its first and second derivatives. Upper row) reference profile. Middle row) first derivatives of the reference profile. Lower row) second derivatives of the measured attenuation profile.

A sliding window technique was used to find the best shift parameter x_0, while a brute force search was used to find the best matching reference attenuation profile f_t. Once the best matching attenuation reference profile was found, both the location and thickness of the airway walls were determined using the shift parameter x_0 and thickness parameter t, respectively, for the given angular sample of measured attenuation profile g.

It was the purpose of estimating two airway dimension parameters, namely the airway wall thickness *WT* and the lumen diameter *LD* of the given ROI. To this end, the above procedure was repeated for the 72 angular samples of the measured attenuation profiles from the given ROI. The wall thickness *WT* of the given ROI

was determined as the average thickness t obtained from each profile sample that passed certain quality criteria. The lumen diameter *LD* was determined as the averaged length from the ROI centre to the wall transition point of the matched ideal profile I_t.

Figure 14 illustrates an example of the attenuation profile matching procedure.

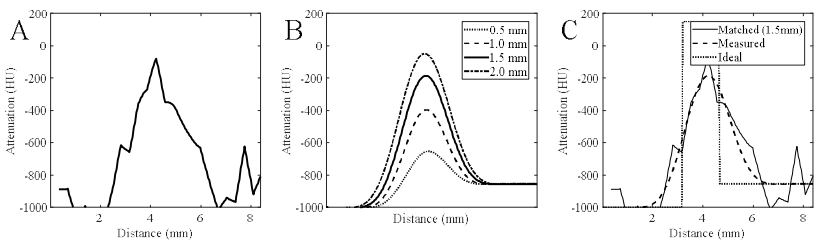

Figure 14. Illustration of an example of our attenuation profile matching procedure. The acquisition of a measured attenuation profile (A) triggers the generation of the 7reference attenuation profile set (B), which in turn leads to the determination of the best matching reference profile and its ideal counterpart (C).

With residual error, the results in matching range were shown as accurately matched. In COPDgene phantom, the errors of each angle were relatively flat, which indicates the peak position, range and intensity of each area were correctly set. In patient image case, there were some residual errors found in relatively thicker object area – which can be referred as thicker airway wall or vessel attached area, since the maximum estimation range was set to 2.5 mm. Figure 15 showed the residual map of the intermediate result in measuring the tubes in the COPDgene phantom. Figure 16 showed the sample residual map of the intermediate result in measuring the patient airway.

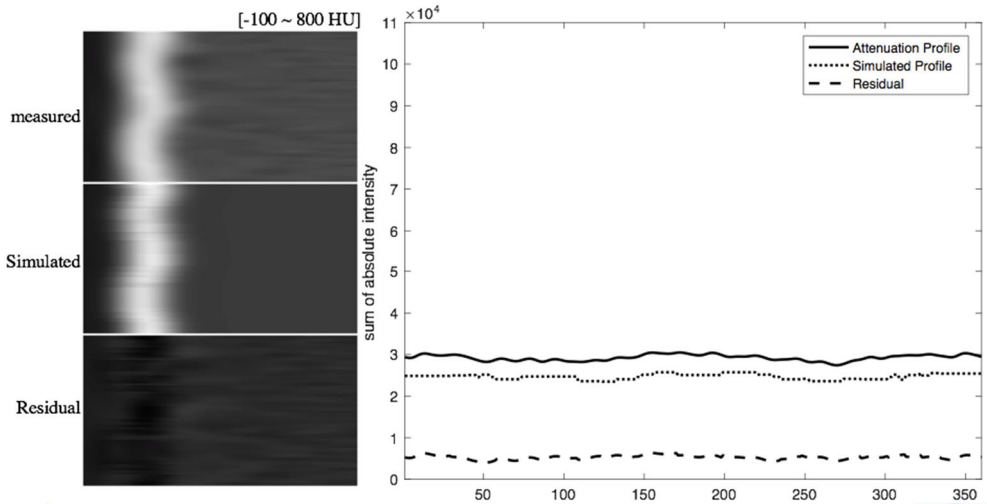

Figure 15. Residual map and the residual error plot of the airway tube of the COPDgene phantom. Results were shown as flat.

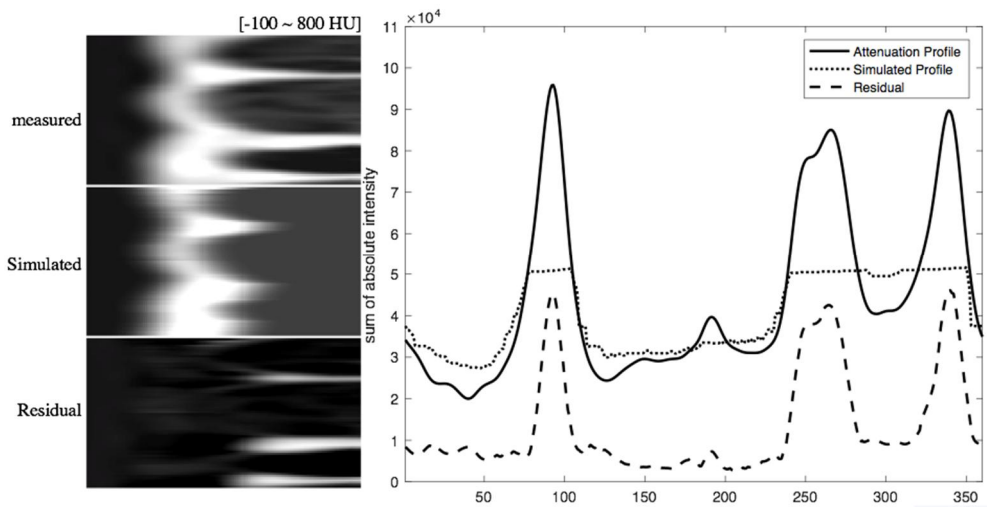

Figure 16. Residual map and the residual error plot of the airway of the patient image. Some residual errors were found in the thicker object.

3.5 Quality Control

A quality control (QC) procedure was designed to ensure the reliability of the estimated airway dimensions.

The QC checkpoints were placed in two steps. The first checkpoint was placed to assess the matching error of each angular-sampled attenuation profile. It was checked if the minimum weighted distance E_{min} exceeded the predefined tolerance criteria, which was set to two times the standard deviation of the noise measured on the ROI on a uniform soft tissue area. The profiles that did not pass the first checkpoint were rejected for further use.

The second checkpoint was to assess the quality of the two fitting parameters, t and x_0, from each profile to determine their appropriateness in use for estimating *WT* and *LD*. At this step, the histogram of each parameter t and x_0 was created and fitted to a mixture of *N* Gaussian curves using the EM algorithm,[54] in which the number of Gaussian curves was set to vary from 1 to 3. Then, the parameter values for t and x_0 that belonged to the first Gaussian were accepted, while the rest were rejected.

This QC process reflects our findings from a preliminary experiment. Often, attenuation profiles across the airway wall attached to a high-intensity structure resulted in outlier values for the fitting parameters, which caused large errors in the measured airway dimensions if not filtered out properly. Therefore, the first checkpoint was intended to reject those attenuation profiles across the airway walls attached to high-intensity structures.

More often than not, the cross-section of an airway appears to have an elliptical rather than circular shape. Our finding was that an ROI on a circular airway results

in a unimodal Gaussian-like histogram of wall dimension parameters, while an ROI on an elliptical airway results in a multi-modal histogram. In addition, in cases where the wall dimension parameters from an ROI made a multi-model histogram, the wall dimension parameters belonging to the first peak of the histogram were observed to correspond to the attenuation profile group sampled near the short axis of the ellipse, which resulted in sufficiently accurate airway dimension values.

Therefore, the second checkpoint corresponded to selecting the suitable part of the attenuation profile samples near the short axis of the ellipse. In cases in which the ROI was put on a circular airway, the second checkpoint accepts the wall dimension results from all attenuation profiles. Figure 18 compares the intermediate results of the QC procedure from ROIs on example airway cross sections for a vessel-attached airway (A-C) and a tilted airway (D-F)

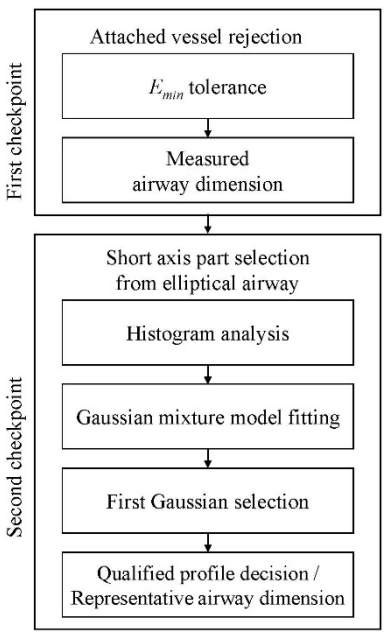

Figure 17. Schematic diagram of the quality control procedure. The first checkpoint rejects the attenuation profiles of airway walls attached to neighbouring blood

vessels, and the second checkpoint selects the suitable part of the attenuation profile samples near the short axis from the elliptical cross-section of a tilted airway.

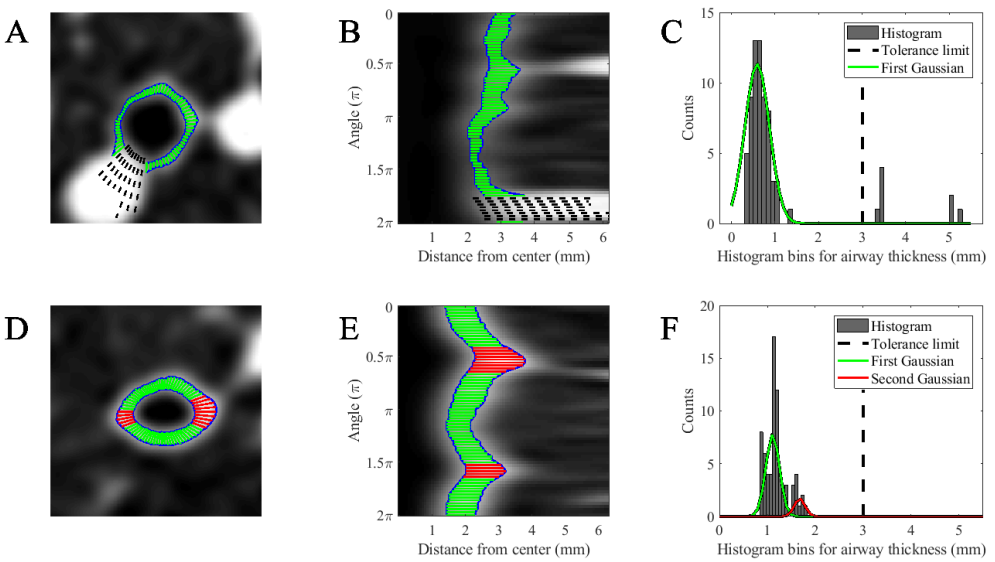

Figure 18. Intermediate results of the QC procedure from ROIs on example airway cross sections for a vessel-attached airway (A-C) and a tilted airway (D-F). A and D show the angular samples of attenuation profiles overlaid on ROI subimages with pseudocolours where the dashed black lines and red lines represent the rejected attenuation profiles at the first and second checkpoints, respectively, the green lines represent the accepted ones, and the blue curves represent the estimated airway wall contours. B and E are stack representations of the angular sampled attenuation profiles. C and F show the histogram plots for the estimated wall thickness of attenuation profiles with an overlay of the derived Gaussian mixture model. Here, the tolerance limit at the first checkpoint was set to 3.0 mm, and the attenuation profiles belonging to the 1st Gaussian were only accepted at the second

checkpoint for subsequent use.

3.6 Performance Evaluation with a Phantom

A phantom study was carried out to evaluate the performance of the proposed method in terms of measurement accuracy and robustness against varying scan parameters and airway tilts. Measurement accuracy was evaluated for four non-tilted airway tubes of varying sizes. The FWHM method was used as a reference for performance comparison.

The Scan parameter-robustness of the APM method was evaluated against the four scan parameters, such as reconstruction kernel, radiation exposure, FOV, and slice thickness. Tilt-robustness was evaluated by comparing the *WT* accuracies obtained for the tubes of the same size with and without tilt.

For the evaluation of the scan parameter-robustness of our method, the variation of the mean error in the *WT* measurements for the four non-tilted tubes was assessed with the scan parameter of interest being changed while the remaining scan parameters remained constant. Details of the scan parameter settings used for the robustness evaluation against each scan parameter are listed in Table 4.

Table 4. Scan parameter settings used for the evaluation of robustness against each scan parameter. The bold texts represent the range of parameter values were changed, while the plain texts denote the fixed settings used.

Scan parameter of interest	Scan Parameter Combinations			
	Kernel	Dose	Slice Thickness	FOV
Kernel	**B10s–B80s**	200 mAs	0.75 mm	180 mm
Dose	B30s	**25, 100, 200 mAs**	0.75 mm	180 mm
Slice Thickness	B30s	200 mAs	**0.75, 1.5, 2.25, 3 mm**	180 mm
FOV	B30s	200 mAs	0.75 mm	**180, 250, 320, 400 mm**

3.7 Pilot Clinical Test 1: Wall thickness comparison analysis between COPD / Normal subjects

To evaluate the feasibility of the proposed APM method for clinical use, a pilot clinical test was performed with a small patient dataset. Twenty patient CT studies were obtained from the Seoul National University Hospital. Among them, 10 patients were COPD patients, while the rest were normal subjects.

The scan conditions were 120 kVp, 40 mAs, 1-mm thickness, and B30s reconstruction kernel. An airway of interest was selected for measurement at the fourth branch of the airway from each case using a 3D interactive rendering of the segmented airway as visual guidance. Shown in Figure 19 are an example ROI and the corresponding 3D rendering of the segmented airway.

It was essential to get the accurate the centre position of the selected airway since the strayed centre might cause the distorted sampling track line. The centre of

the airway is selected automatically by calculating the centre of mass of the segmented lumen area. Adaptive threshold method was used for segmentation of selected lumen area.

Airway branch labels correspond to the division of the lung into compartments: LMB and RMB lead to the left and right lungs; LUL, RUL, L4+5, R4+5, LLB, RLL lead to the lobes; and R1-R10, L1-L10 lead to (up to) 10 segments in each lung.[18,55]. Moreover, for the unbiased manual selection of the human operator, simple selection criteria were defined. The airway should be tubular/elliptical shaped[13,18] with full-closed circle, relatively round, visible in CT axial slice, being exist at 3rd/4th branch or latter[24], and as possibly in meaningful range in clinically significant, such as following the definition of the AWT-Pi10[28,56], which is the definition of the airway wall thickness at internal perimeter as 10 mm.

Table 5 showed the selected branch positions of the airway from each patient, and their FEV1/FVC value. Each branch positions were indicated as airway labels.

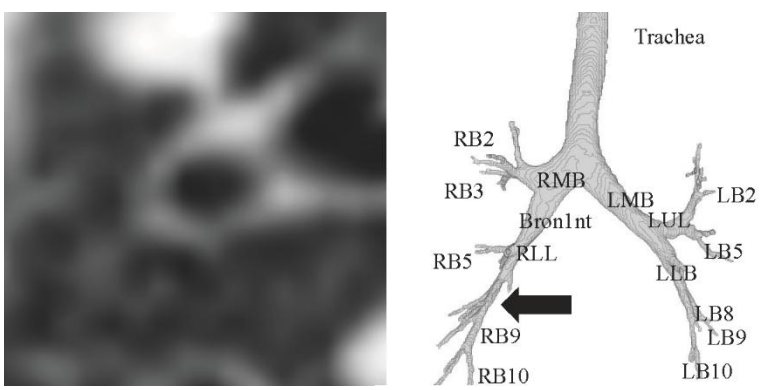

Figure 19. Example ROI image and segmented airway of a patient case selected for use in the pilot clinical test. The target airway position was selected at the third or fourth branch (RB5, RB3, LB2, LB5, etc.).

Table 5. Selected branch positions of the airway from each patient, and FEV1/FVC value. Each location in normal group was selected randomly, and thickened airway was intentionally selected in the COPD group.

Normal group			COPD group			
Patient No	Selected position	FEV1/FVC	Patient No	Selected position	FEV1/FVC	Misc.
NORMAL 1	RB2,RB3,LB 5,LLB	77%	COPD 1	RB3,RLL,LB 5	64%	Airway thickening in upper lobe
NORMAL 2	RB3,RB5,LB 5,LB9,LB10	79%	COPD 2	RB3,LLB,LB 8	61%	Airway thickening in upper lobe
NORMAL 3	RB5,LB5	78%	COPD 3	RB2,LUL,LB 5	61%	Airway thickening
NORMAL 4	RB5,RB9,LB 10	77%	COPD 4	RB3,LB5,LB 9	58%	Airway thickening in lower lobe
NORMAL 5	RB5,RB9,LB 5,LB8	70%	COPD 5	RB5,LB5	59%	Airway thickening
NORMAL 6	RB2,RB4+5, LB5	81%	COPD 6	RLL,LB5	53%	Air trapping
NORMAL 7	RB2,RB9,LB 5	87%	COPD 7	RB9,LB5	67%	Airway thickening
NORMAL 8	RB5,RB9,LB 9,LB10	85%	COPD 8	RB3,LB2,LL B	67%	Bronchititis
NORMAL 9	RB2,RB9,LL B,LB9	75%	COPD 9	RB3,RB8,LB 5,LLB	69%	Airway thickening
NORMAL 10	RB2,RLL,LB 5	83%	COPD 10	RB2,RB9,LB 4+5,LLB	65%	Airway thickening in upper lobe

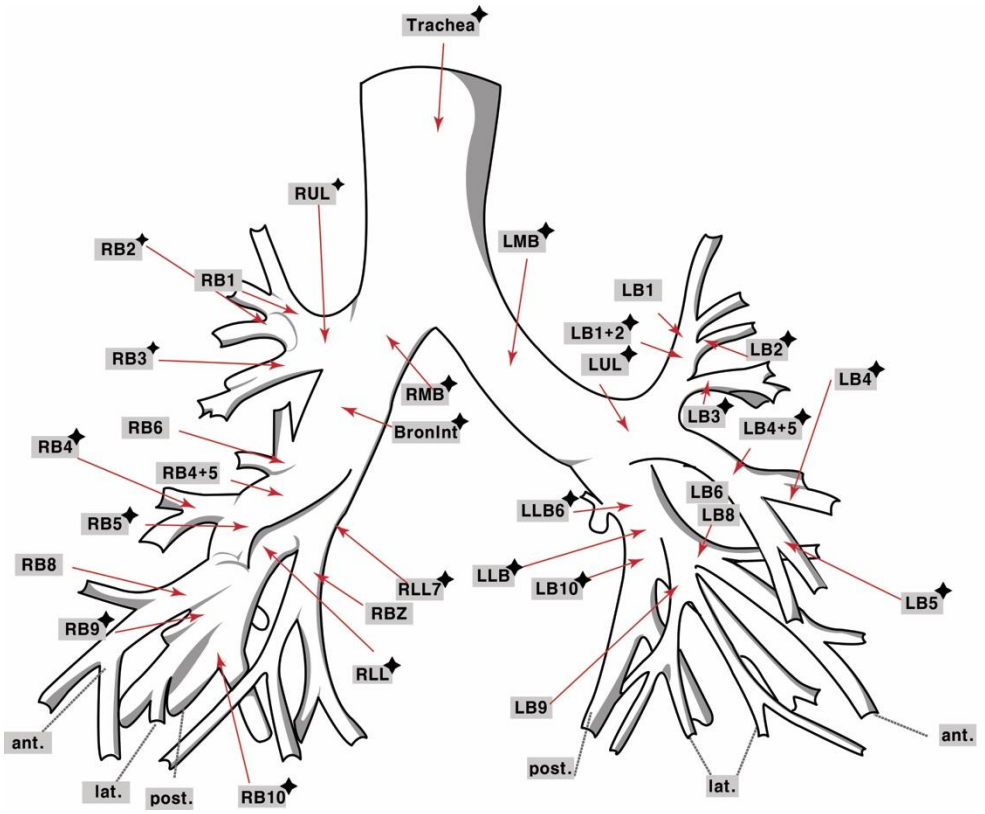

Figure 20. The label of the airway tree. The drawing is redrawn based on various literatures[18,55,57].

3.8 Pilot Clinical Test 2: Wall dimension changes between inspiration/expiration

Airway size and wall thickness may vary depending on inspiration level, However, the changes in wall thickness measurement may give a misleading information. How much they change during patient breathing remains still ambiguous. To evaluate the additional feasibility of the proposed APM method.

Ten normal subjects were acquired from Seoul National University Hospital, with a commercial CT (Sensation 16, Siemens) At inspiration and expiration

conditions, With low-dose CT scan condition. (120kVp, 40mAs, and 1mm slice thickness, B30f kernel)

In each dataset, 2 small airways at 3rd to 4th generation bronchial segments (RB5, RB3, LB2, LB5, etc.) were selected and matched between inspiration and expiration CT scans with visual assessment. Each selected airway was sampled with 72 angular samples of measured attenuation profiles from the given ROI, covering 360 degrees.

Table 6. Selected branch positions of the airway from each patient. Each location in normal group were selected randomly, and their positions were matched manually.

Patient No	Patient No	Patient No	Selected position
INSP 1	RB3,LB5	EXP 1	RB3,LB5
INSP 2	RB3, RB9	EXP 2	RB3, RB9
INSP 3	RLL, LB5	EXP 3	RLL, LB5
INSP 4	RB7, LLB	EXP 4	RB7, LLB
INSP 5	RB9, LLB	EXP 5	RB9, LLB
INSP 6	RB5, LB5	EXP 6	RB5, LB5
INSP 7	RB5, LB5	EXP 7	RB5, LB5
INSP 8	RB5, LB5	EXP 8	RB5, LB5
INSP 9	RB9, LB4+5	EXP 9	RB9, LB4+5
INSP 10	RB7, LB9	EXP 10	RB7, LB9

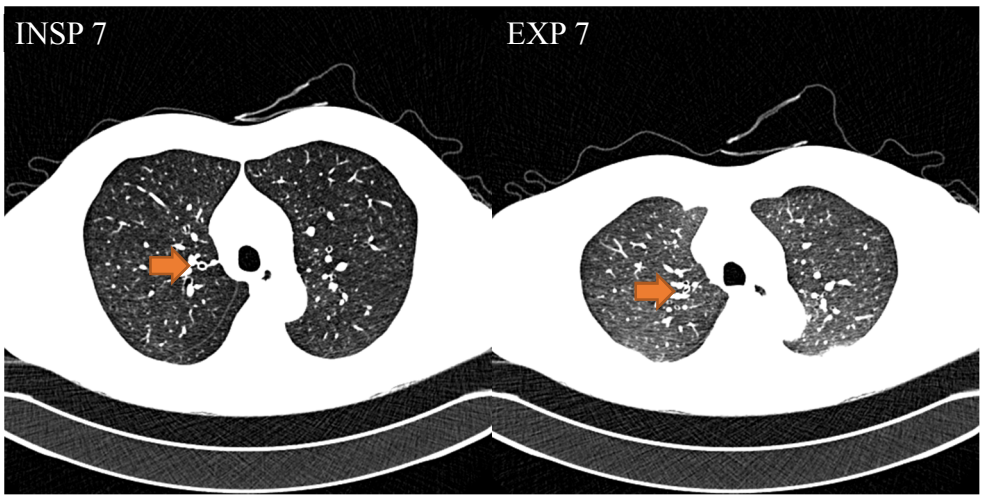

Figure 21. One of the CT image pair of the pilot patient case. Same airway position along the inspiration and expiration was selected manually.

4. RESULTS

4.1 Phantom study

The measurement of the proposed method in COPgene phantom case were shown in figure 22 and figure 23. The overall measurement accuracy of the *WT* assessed with the non-tilted airway tubes in the phantom study was compared for the APM and FWHM methods, as shown in Figure 24 and Table 7. Measurement statistics were drawn from the pooled measurements for a total of 384 combinations of scan parameters. Wall thickness measurements obtained with the APM method showed no bias for either of the four airway tubes, while those obtained with the FWHM method were consistently accompanied by a positive bias ranging from 0.16 to 0.87 mm. Overall, the APM method produced mean error values in a considerably smaller range (0.02 to 0.04 mm) compared to that of the FWHM method (0.26 to 0.72 mm). Specifically, the mean error for the 0.6-mm-thick airway tube (Tube No. 2) obtained with APM method was 0.02 mm (3.33%), which showed sharp contrast with the mean error of 0.72 mm (120%) obtained with the FWHM method.

When comparing the distribution of *WT* measurements for the 0.6-mm-thick and 0.9-mm-thick tubes shown in Figure 24, it is evident that the APM method allows for a clear distinction between the two tubes, whereas the measurements obtained with the FWHM method overlap substantially and are thus barely distinguishable from each other.

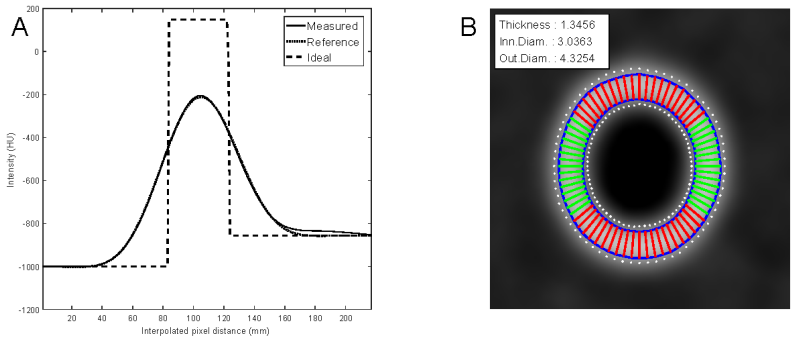

Figure 22. Right) the plot result of the proposed method, Left) ROI of the COPDgene phantom CT image. The tube was tilted 30 degrees along the axis. The short axis was successfully ranged from QC process. Tube wall thickness was 1.2 mm.

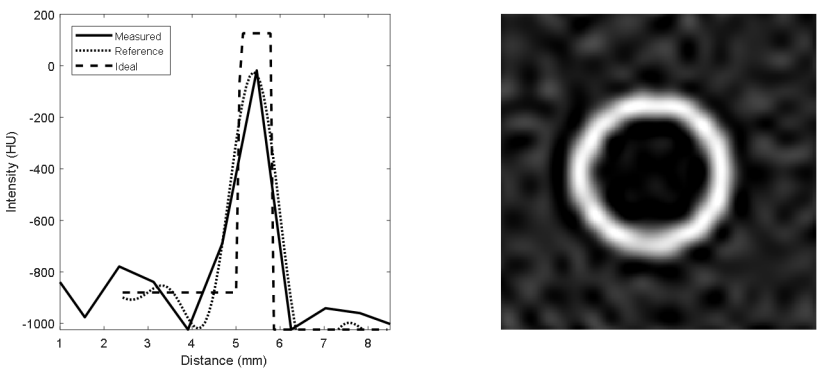

Figure 23. Right) the plot result of the measured attenuation profile, matched reference profile, and its ideal profile. Left) ROI of the COPDgene phantom image with relatively high noise. Overlay of the result was not displayed on purpose of showing the noise of the image. Tube wall thickness was 0.9 mm and scanned at 25mAs exposure. B50s kernel was used to reconstruct the image.

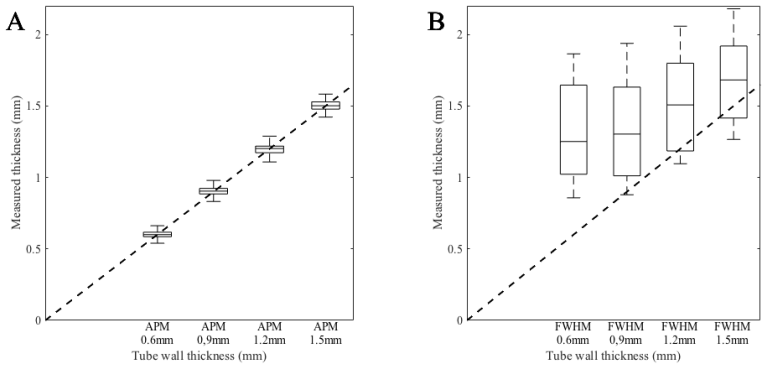

Figure 24. Box plots compare the overall accuracy of the wall thickness measurements obtained in the phantom study for the non-tilted airway tubes with (A) the APM method and (B) the FWHM method. While the measurements for the 0.6 and 0.9 mm tubes obtained with APM method show clear distinction, those obtained with the FWHM method overlap substantially and are barely distinguishable from each other.

Table 7. Overall accuracy of the WT measurements for the non-tilted airway tubes in the phantom study. Statistic data were drawn from the pooled measurements for a total of 384 combinations of CT scan parameters.

Tube No.	*WT* (mm)	Mean (mm)	Std. dev. (mm)	Bias (mm)	Mean error (mm)
APM method					
2	0.6	0.60	0.03	0.00	0.02 (3.33%)
3	0.9	0.90	0.05	0.00	0.03 (3.33%)
5	1.2	1.20	0.05	0.00	0.04 (3.33%)
6	1.5	1.50	0.08	0.00	0.04 (2.67%)
FWHM method					
2	0.6	1.32	0.32	0.72	0.72 (120%)
3	0.9	1.32	0.33	0.42	0.42 (46.7%)
5	1.2	1.48	0.32	0.28	0.31 (25.8%)
6	1.5	1.66	0.28	0.16	0.26 (17.3%)

The overall measurement accuracies for *LD* obtained with the non-tilted airway tubes in the phantom study using the APM and FWHM methods were compared, as shown in Table 8. Overall, the APM method produced mean error values in a smaller range (0.15 to 0.17 mm) compared with that of the FWHM method (0.31 to 0.65 mm). In particular, the *LD* measurements for the smallest airway tube (3-mm LD) obtained with the APM method had a negligible bias (−0.05 mm, −1.67%), while those obtained with the FWHM method had a substantial amount of negative bias (−0.65 mm, −21.67%).

Table 8. Overall accuracy of the *LD* measurements for the non-tilted airway tubes in the phantom study. Statistic data were drawn from the pooled measurements for a total of 384 combinations of CT scan parameters.

Tube No.	*LD* (mm)	Mean (mm)	Std. dev. (mm)	Bias (mm)	Mean error (mm)
APM method					
2	3	2.95	0.24	-0.05	0.17 (5.67%)
3	6	5.82	0.30	-0.18	0.24 (4.00%)
5	6	5.83	0.41	-0.17	0.27 (4.50%)
6	6	6.07	0.16	0.07	0.15 (2.50%)
FWHM method					
2	3	2.35	0.36	-0.65	0.65 (21.67%)
3	6	5.82	0.36	-0.18	0.33 (5.50%)
5	6	5.97	0.37	-0.03	0.34 (5.67%)
6	6	6.12	0.33	0.12	0.31 (5.17%)

4.2 Human pilot study

The robustness results of the *WT* measurements obtained with APM method against the four CT scan parameters are illustrated using box plots in Figure 25 and are represented in Tables 9 to 12.

The kernel robustness results are shown in Figure 25A and Table 9. The APM method tended to exhibit a smaller error in the wall thickness measurement for smoother kernels (B10s–B40s; 0.01 to 0.02 mm) than for sharper kernels (B50s–B80s; 0.03 to 0.05 mm). In general, the APM method was observed to be robust to varying reconstruction kernels in CT scans with a relative error lower than 8.33%.

The robustness results against the remaining three scan parameters (radiation exposure, FOV, and slice thickness) are shown in Figure 25B–D and Tables 10 to 12. The APM method was observed to also be robust to those three scan parameters. The error range of these measurements remained consistent regardless of the scan parameter changes for the four tube sizes. For example, the mean error of the *WT* measurements of Tube 2 did not change despite the reduction of radiation exposure from 200 to 25 mAs. Neither the changes in FOV from 180 to 400 mm nor the changes in slice thickness from 0.75 to 3.0 mm affected the mean error of the *WT* measurements for the same tube.

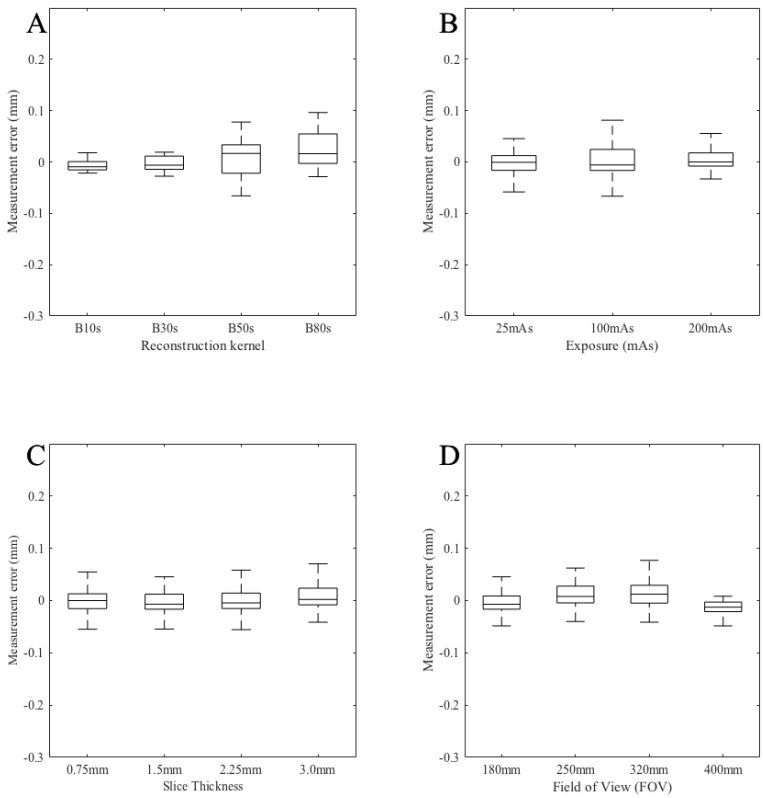

Figure 25. Box plots show the robustness results of the APM method against varying (A) reconstruction kernels, (B) radiation exposure, (C) slice thickness, and (D) FOV. The variation of the WT measurement error for Tube 2 (0.6-mm thick, non-tilted) was assessed to represent the robustness of the method. Statistic data were drawn from the pooled measurements for a total of 384 combinations of CT scan parameters.

Table 9. Robustness of the APM method against varying reconstruction kernels as assessed by the variation of the mean error (mm) in the wall thickness measurements of the non-tilted airway tubes. Statistic data were drawn from the

pooled measurements for a total of 384 combinations of CT scan parameters.

Tube No.	Reconstruction Kernels							
	B10s	B20s	B30s	B40s	B50s	B60s	B70s	B80s
2	0.01	0.01	0.01	0.02	0.03	0.03	0.03	0.03
3	0.02	0.01	0.02	0.03	0.03	0.03	0.05	0.07
5	0.01	0.01	0.02	0.02	0.04	0.04	0.07	0.10
6	0.02	0.02	0.02	0.03	0.04	0.06	0.07	0.06

Table 10. Robustness of the APM method against radiation exposure as assessed by the variation of the mean error (mm) in the wall thickness measurements of the non-tilted airway tubes. Statistic data were drawn from the pooled measurements for a total of 384 combinations of CT scan parameters.

Tube No.	Radiation Exposures (mAs)		
	25	100	200
2	0.02	0.03	0.02
3	0.03	0.03	0.03
5	0.04	0.04	0.03
6	0.05	0.03	0.04

Table 11. Robustness of the APM method against FOV as assessed by the variation of the mean error (mm) in the wall thickness measurements of the non-tilted airway tubes. Statistic data were drawn from the pooled measurements for a total of 384 combinations of CT scan parameters.

Tube No.	FOV (mm)			
	180	250	320	400
2	0.00	0.00	-0.01	0.00
3	0.00	0.00	0.00	0.01
5	0.00	0.01	0.00	-0.01
6	0.01	0.01	0.00	0.02

Table 12. Robustness of the APM method against slice thickness as assessed by the variation of the mean error (mm) in the wall thickness measurements of the non-tilted airway tubes. Statistic data were drawn from the pooled measurements for a total of 384 combinations of CT scan parameters.

Tube No.	Slice Thickness (mm)			
	0.75	1.5	2.25	3.0
2	0.00	0.00	-0.01	0.00
3	0.00	0.00	0.00	0.01
5	0.00	0.01	0.00	-0.01
6	0.01	0.01	0.00	-0.02

The robustness results against tilt angle are shown in Table 13. The mean error in the *WT* measurements increased slightly from 0.02 (3.33%) to 0.05 (8.33%) mm and from 0.04 (3.33%) to 0.06 (6.66%) mm as the tilt angle changed from 0 to 30 degrees for the 0.6 and 1.2 mm-thick tubes, respectively. The variation of measurement error due to airway tilt angle was comparable to that caused by scan parameter changes.

Table 13. Robustness of the APM method against tilt angle as assessed by the variation of the mean error (mm) in the WT measurements. Statistic data were drawn from the pooled measurements for a total of 384 combinations of CT scan parameters.

Tube Thickness	Tilt Angle (degree)	
	0	30
0.6 mm	0.02	0.05
1.2 mm	0.04	0.06

In Figure 26, the colour overlays of the airway dimension measurements for the normal and COPD subjects obtained with the APM and FWHM methods are compared. The airway wall contours extracted with the APM method (blue) appear to be consistently narrower than those obtained with the FWHM method (yellow) for both normal and COPD subjects. Moreover, the thickening of airway walls, as well as the enlargement of LD in the COPD patients compared with those in normal subjects, can be easily discerned. The coloured segments in green and red represent the accepted and rejected angular samples, respectively, in the quality control steps. The successful operation of the QC steps of the APM method for both normal and COPD subjects can be appreciated. The QC function worked successfully for varying shapes of airways, including moderately circular shapes (A and D), elongated shapes (B and E), and airways with strong vessel attachment (C and F).

WT measurements from the pilot clinical cases are compared in Figure 27 for the APM and FWHM methods. The box plots for the APM method results shown in Figure 27A show a clear distinction between the wall thickness measurements obtained from normal subjects (0.6 mm ± 0.2) and COPD subjects (1.1 mm), with a substantial increase (80%) for the latter patients. In contrast, the box plots for the FWHM method results shown in Figure 27B mostly overlap for the measurements from both normal and COPD subjects, and thus fail to show any distinction.

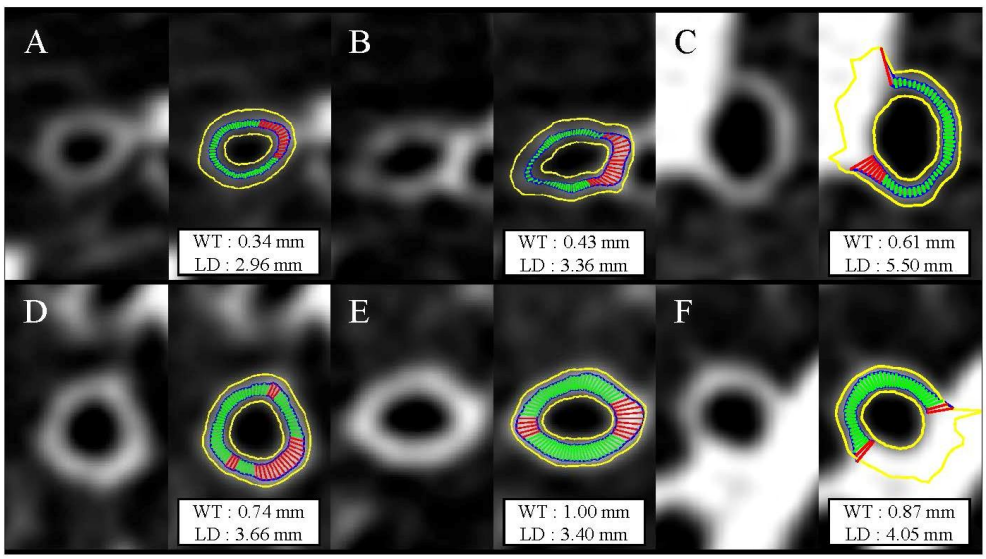

Figure 26. Example results of airway wall thickness and lumen diameter measurements for selected airways from normal (A, B, C) and COPD (D, E, F) subjects. For comparison purposes, original and colour overlaid images are shown at the left and right sides, respectively. WT and LD represent the measured wall thickness and the lumen diameter obtained with the proposed method, respectively. Yellow and blue curves represent the airway wall contours extracted with the FWHM and APM methods, respectively. The green and red segments represent the accepted and rejected angular samples, respectively, at the QC steps of the APM method. The successful operation of QC procedure for airways with a moderately circular shape (A and D), with an elongated shape (B and E), and with strong vessel attachment (C and F) can be appreciated.

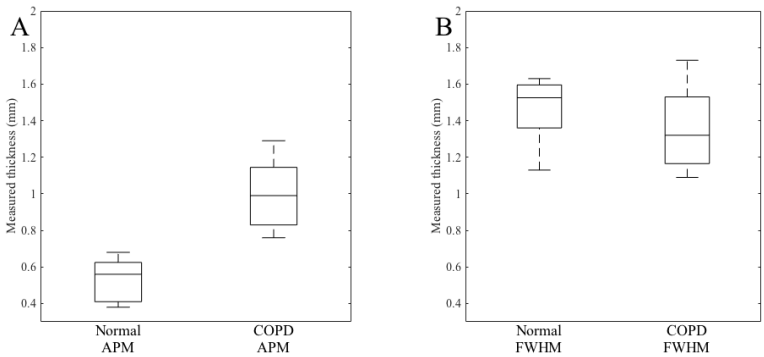

Figure 27. Box plots compare the WT measurements from the pilot clinical cases for normal and COPD subjects obtained with (A) the APM and (B) the FWHM methods

Figure 28 shows the colour overlays of the airway dimension measurements for the for the inspiration and expiration of the lung. The difference in the results between intake and exhalation and the lumen diameter was varied in each case. In figure 28A show a significant difference of the lumen diameter and wall thickness. In figure 28B, the wall thickness of the airway showed a moderate difference while lumen diameter difference was unremarkable. Figure 28C showed somewhat mixed result, the difference of the lumen diameter showed significant change, but the airway wall thickness was not much varied comparing the other cases. It is assumed that the blood flow might affect to the airway wall since the airway was relatively close to the heart.

Table 14 showed the summary of the second pilot clinical test. Figure 29 showed the box plot result of the inspiration and expiration. Average airway wall thickness was increased from 0.67 ± 0.21 mm in inspiration, to 0.91 ± 0.23 mm in expiration. (44%) The measurement variability for the thickness of each airway

wall is considerable, indicating that there is a variability in thickness for each airway's characteristics.

In Figure 30, the result of the lumen diameter and the outer diameter between inspiration and expiration were shown in the boxplot. The lumen diameter between inspiration and expiration showed some significant differences, while the outer diameter showed relatively modest differences.

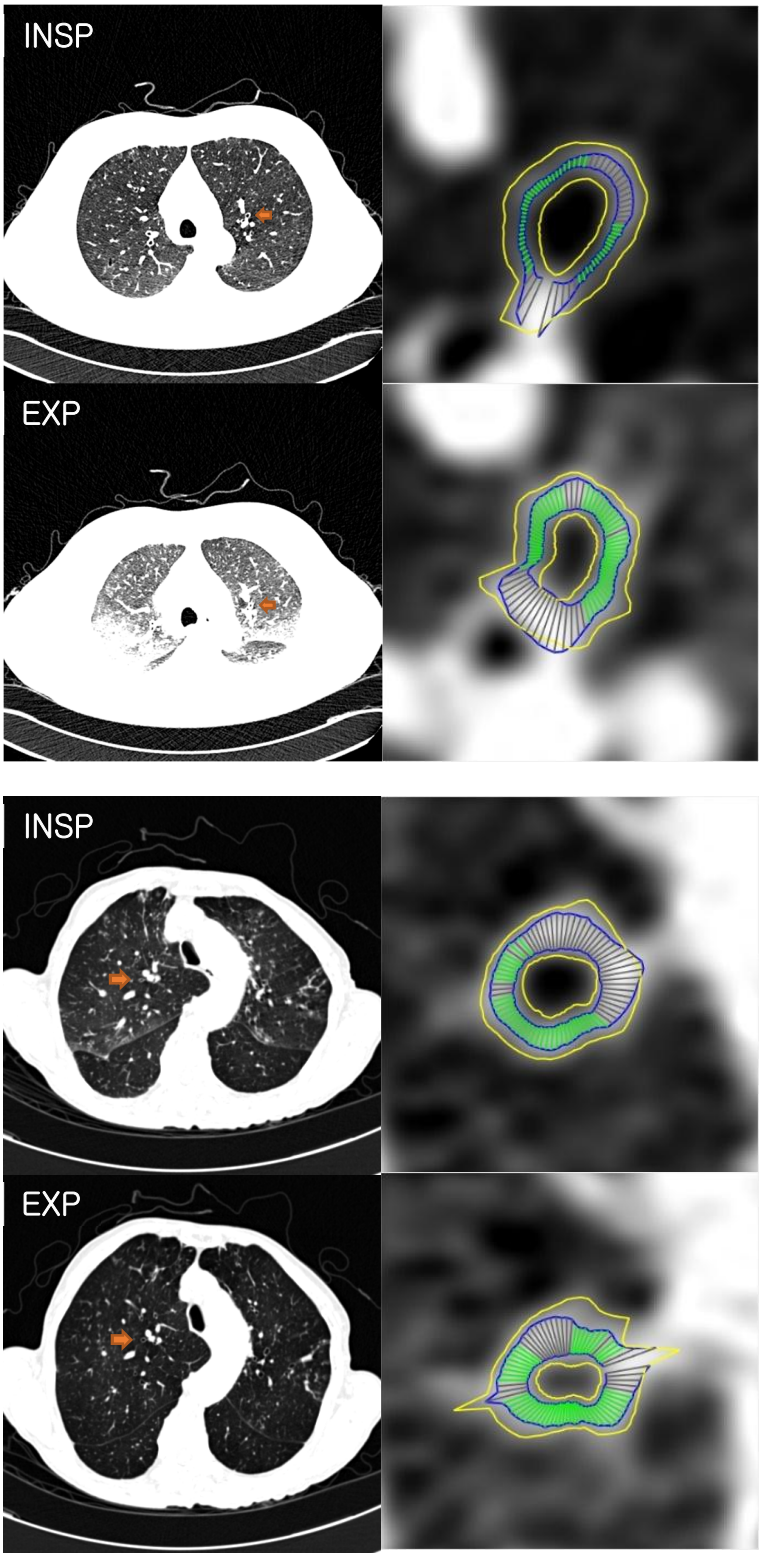
INSP
EXP
INSP
EXP

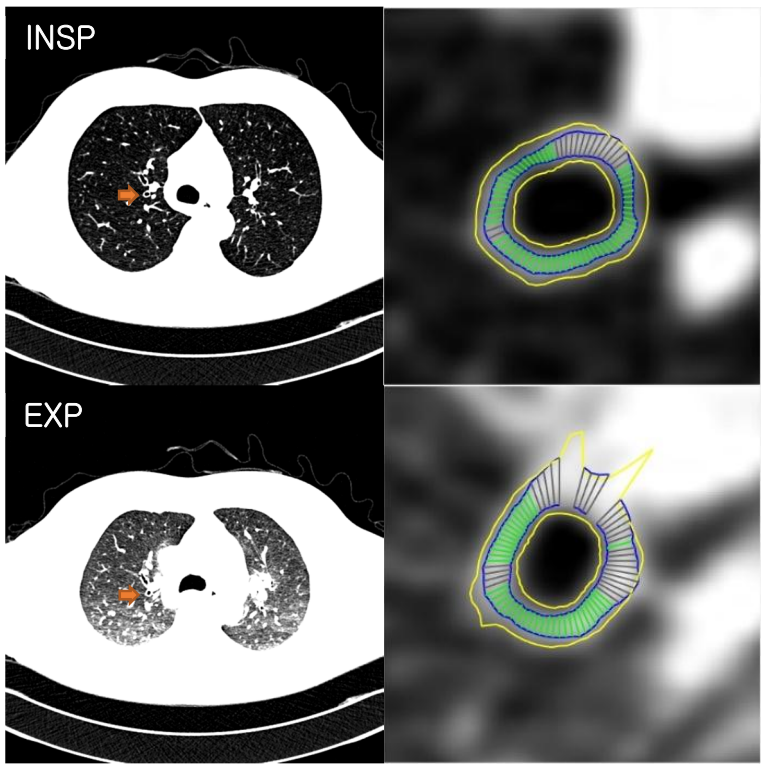

Figure 28. Example results of airway wall thickness and lumen diameter measurements for selected airways from inspiration (upper row) and expiration (lower row). For comparison purposes, original CT image and colour overlaid images are shown at the left and right sides, respectively. The green and grey segments represent the accepted and rejected angular samples, respectively, at the QC steps of the APM method.

Table 14. Overall measurements of the inspiration and expiration of the lung.

	Mean	Std.	1st Quan.	3rd Quan.
Inspiration	0.67 mm	0.21 mm	0.47 mm	0.73 mm
Expiration	0.91 mm	0.23 mm	0.67 mm	0.90 mm
Abs. Difference	0.32 mm	0.13 mm	0.23 mm	0.42 mm
Coefficient of Variance	44%	38%	-	-

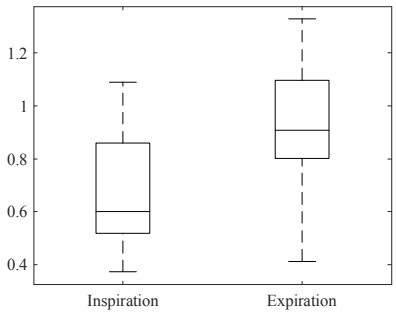

Figure 29. Box plot result of the measurement for the inspiration and expiration of the pilot patient case. The difference between the inspiration and the expiration showed discriminately.

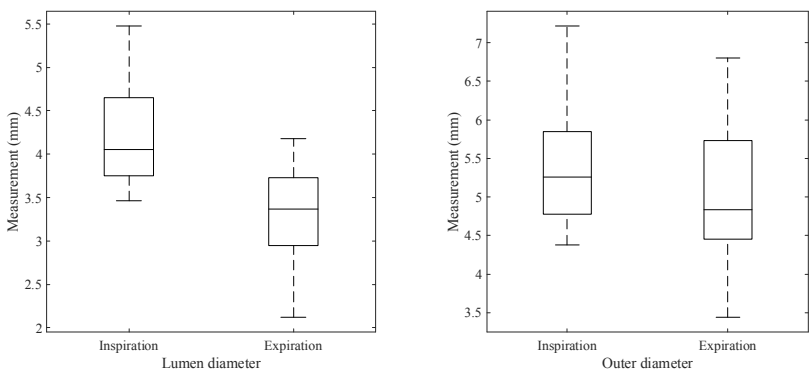

Figure 30. Box-plot result of the measurement difference between the inspiration and expiration of the pilot patient case. Expiratory group showed higher difference between the lumen diameter and outer diameter, while the outer diameter did not show the significant difference.

5. DISCUSSION

Limitations in accuracy and reliability in the measurement of small airway dimensions via CT have remained as a crucial bottleneck in bringing the advanced imaging capability of CT into clinical reality. A number of studies have pointed out the importance of the accurate assessment of small airway dimensions via CT because it could allow for the characterization of small airway remodelling, which is responsible for airflow limitations and gas-exchange dysfunctions in COPD patients.[31,33,58,59] Despite continued study efforts, however, the accuracy and reliability in the measurement of small airway dimensions via CT have remained dependent on the CT systems and the imaging conditions used. As concerns over CT radiation dose continues to grow, the scan parameters in follow-up imaging sessions are likely to change, following a direction in which radiation dose is further reduced. Therefore, the motivation of our study was to develop a novel method which allows for accurate and reliable measurements of small airway dimensions with robustness against varying scan conditions.

In this study, a novel APM method was designed that employs the point spread function of a CT system. I assumed that our proposed APM method could yield better accuracy and reliability, especially in low-dose CT settings, because it takes into account diverse factors affecting the measurement accuracy of airway dimensions, including reconstruction kernels, image noise, differing recon FOV, and slice thickness; these factors were recognised to compromise the accuracy in the measurements of airway dimensions in previous studies.

In our phantom study, it was evaluated that the performance of our method in

terms of robustness against varying scan parameters and accuracy in determining airway dimensions. Our proposed APM method consistently exhibited high accuracy for varying scan parameters, including eight reconstruction kernels, three radiation dose levels, four slice thicknesses, and four FOV conditions.

More importantly, for the smallest air tubes with a wall thickness of 0.6 mm and a lumen diameter of 3 mm, the mean error in wall thickness measurements was as low as 0.02 mm and remained the same even at the lowest dose condition (25 mAs). This indicates that the APM method has the potential to provide accurate measurements of airway dimensions for small airways, especially in low-dose CT scans. Considering study reports pointing out that the major bottleneck in CT-based quantification of airway abnormality lies in the limitations of the measurement accuracy of small airways, the performance of the APM method shown in this study is expected to make an important contribution towards advancing the role of CT in the quantitative characterization of the imaging phenotype of COPD.

In this study, 'small airways' was referred to those with an internal diameter of less than 2–3 mm, following a broad definition of small airways.[14,39,60] However, there also exists a strict definition of small airways, indicating that they are those with an internal diameter <2 mm.[15] In this regard, our study is limited for not presenting the performance for airway tubes falling under the strict definition of 'small' airways. A further study is warranted to validate the performance of the proposed APM method with a new phantom containing airway tubes that adhere to the strict definition of small airways.

To the knowledge of the author, our study introduced the experimentally acquired PSFs to the measurement of airway wall dimensions for the first time.

Previous studies often employed a hypothetical Gaussian shaped PSF in an attempt to maximize the accuracy of airway dimension measurements, and showed an improved accuracy with an experiment with a specific CT system.[12,24] In reality, however, it is uncertain exactly which reconstruction kernels really follow a Gaussian shape. For example, most sharp kernels contain overshoots and undershoots which do not follow a Gaussian shape at all. In contrast, our study took an approach employing experimentally acquired PSFs, and therefore has the advantage of being applicable to a variety of reconstruction kernels used in different CT scanners. The consistent high accuracy of our method over the varying reconstruction kernels shown in our results is mainly attributable to the use of those experimentally acquired PSFs.

A key strength of the proposed APM method is that it requires neither complex 3D image analysis procedures nor thin-slice 3D imaging data. The majority of advanced airway dimension measurement techniques proposed in previous studies are 3D-based, which require sophisticated procedures, including 3D centre line extraction from the segmented airway, smoothing of the centre line, re-slicing of 3D data onto a plane perpendicular to the centre line, and the determination of cut-off points in an attenuation profile or the modelling of a 3D PSF.[45,61] Various scan parameters, such as slice thickness, FOV, and dose, in principle, may disturb the reliability of 3D processing procedures. In addition, thin-slice image data, which is a prerequisite for 3D-based approaches, comes with much higher image noise, especially when scanned at low-dose levels. These factors make it difficult for 3D-based approaches to overcome the compromise between accuracy and reliability.

In contrast, our proposed APM method is inherently 2D image-based and thus

allows for circumventing many of the problems faced in the previously mentioned 3D image-based approaches. Our study results demonstrate that the APM method is able to provide accurate measurements of small airways consistently over slice thickness ranging from 0.75 to 3 mm, regardless of changes in tilt angle, the reconstruction kernel, FOV, and dose level.

Ideally, a CT image in which the airway was placed perpendicularly to the image plane would make a perfect condition for accurate measurement of the airway dimensions in a 2D image-based approach. In practice, however, it is rare to find such an airway in patient CT images. In reality, instead, airways are usually placed with a tilt from the image plane, and thus they appear as an ellipse sometimes attached to a feeding vessel. Therefore, the selection of the short axis portion of the airway wall was implemented by using an EM technique in our QC step, where a histogram of the wall thickness from each line profile is generated, followed by Gaussian mixture modelling of the histogram. Then the short axis portion was determined by choosing the line profiles belonging to the first Gaussian. The high accuracy of airway dimension measurements in our study results, especially for the tilted airways, appears to support the efficacy of our QC step for overcoming the measurement bias problem associated with the tilted airways in a 2D image-based approach.

These advantages of the APM method allow for wider applications in clinical practice, especially in environments where reduced radiation dose is more favoured. For example, the application of the APM method to low-dose lung screening CT may have great potential for monitoring the changes in airway dimensions of smokers and former smokers at high risk of COPD. Being able to make use of

screening scans in airway studies would be very significant for researchers and clinicians.

One of our motivations for including the measurement of the lumen diameter in the APM method was to estimate the lumen perimeter more accurately in order to determine whether the ROI belonged to the Pi10 category, which is becoming a well-accepted criterion for selecting the ROIs in airway analyses.[62] The APM method was shown to reduce the bias of the lumen diameter measurement for the smallest airway tube from −21.67% to −1.67 % compared with that of the FWHM method. This demonstrates the potential of the APM method for improving the overall measurement accuracy for small airway dimensions. It was noted, however, that the degree of improvement in the accuracy of the measurements of the lumen diameter over that of the FWHM method was not as high as that for the measurements of wall thickness.

There are still a few limitations in our study. Our phantom study included airway tubes only with a single density–and two orientation angles (0 and 30 degrees) due to the limited availability of phantoms. Although this study showed a good performance of the APM method in airway measurements for either orientation angles, a further study is warranted to validate its capability for different tilt angles using a more sophisticated phantom that reflects human airways more faithfully. Moreover, due to the 2D nature of our approach, the APM method has a limitation when measuring airways having a small angle with image plane; the airway cross section may appear extremely elongated, leading to a large error. In the current implementation, the APM method requires a user to select appropriate ROIs and thus the user can reject the selection of such extreme airways.

However, for the implementation of fully automated analysis, an airway selection scheme should be included which takes the airway orientation into account.

A study by Washko et al. raised the question that the CT attenuation profile of an airway wall might be a function of both the wall's thickness and its density, with the latter being affected by inflammatory remodelling.[6,63] In this study, it was not attempted to develop our technique to analyze the wall thickness and the wall density at the same time. Therefore, there is a possibility that the airway walls of the subjects with COPD in this study were made of a mixture of thicker and denser tissue than those of the normal group.

Our study used the CT equipment from a single vendor, and therefore is not readily generalizable for other CT systems. This is especially true for newer CT systems that use iterative reconstruction (IR) techniques. Adding an ability to include the iterative recon CT systems would be a valuable work for widening the utility of the proposed APM method. However, the IRCT systems are known to exhibit non-linear behavior in their PSF. In such systems, the APM technique might need to be modified to apply non-linear PSFs for generating reference attenuation profiles. Currently, however, no established method is available to the best of our knowledge with regard to the measurement of non-linear PSFs in IRCT systems. Therefore, it was left the extension of the APM method to IRCT systems to be the study subject of future research.

In this study, the performance of the APM method was compared with the traditional FWHM method. Although performance comparison with novel airway measurement methods is desirable, It is beyond the scope of this study. A software challenge for airway wall dimensions might be a good opportunity for objectively

comparing the performance among different measurement methods.

This study evaluated the performance of the proposed method mainly with a phantom, and only a small number of patient data was used to show its feasibility in clinical applications. In addition, because the ROI selection was made by a human operator, a selection bias might have been introduced to the measurement of airways from patient CT images. Therefore, an additional study would be necessary to validate the clinical performance of our proposed technique with a larger and well-controlled patient population, including patients with different grades of COPD. Furthermore, in order for our method to be clinically practical, the ROI selection process needs to be automated.

6. CONCLUSION

A novel APM method for the accurate measurement of small airway dimensions was proposed. Our proposed APM method was shown to provide accurate measurements of wall thicknesses with less than 4% error, even for small airway tubes with a wall thickness of 0.6 mm. Our method also showed robustness against varying scan parameters, such as reconstruction kernel, radiation exposure, FOV, and slice thickness, as well as airway tilt angle. Our proposed APM method has the potential to overcome the resolution limitations of current CT systems and determine the small airway dimensions of COPD patients.

REFERENCES

1. Montaudon M, Lederlin M, Reich S, et al. Bronchial Measurements in Patients with Asthma : Comparison of Quantitative Thin-Section CT Findings with Those in Healthy Subjects and Correlation with Pathologic findings. 2009;253(3). doi:10.1148/radiol.2533090303/-/DC1
2. Akinbami LJ, Moorman JE, Bailey C, et al. Trends in asthma prevalence, health care use, and mortality in the United States, 2001-2010. *NCHS Data Brief*. 2012;(94):1-8.
3. Dettmer S, Entrup J, Schmidt M, De Wall C, Wacker F, Shin H. Bronchial wall thickness measurement in computed tomography: Effect of intravenous contrast agent and reconstruction kernel. *Eur J Radiol*. 2012;81(11):3606-3613. doi:10.1016/j.ejrad.2012.04.026
4. Vignola AM, Kips J, Bousquet J. Tissue remodeling as a feature of persistent asthma. *J Allergy Clin Immunol*. 2000;105(6):1041-1053. doi:10.1067/mai.2000.107195
5. Little SA, Sproule MW, Cowan MD, et al. High resolution computed tomographic assessment of airway wall thickness in chronic asthma: Reproducibility and relationship with lung function and severity. *Thorax*. 2002;57(3):247-253. doi:10.1136/thorax.57.3.247
6. Washko GR, Dransfield MT, Estépar RSJ, et al. Airway wall attenuation: a biomarker of airway disease in subjects with COPD. *J Appl Physiol*. 2009;107(1):185-191. doi:10.1152/japplphysiol.00216.2009
7. de Jong PA, Long FR, Nakano Y. Computed tomography dose and

variability of airway dimension measurements: How low can we go? *Pediatr Radiol*. 2006;36(10):1043-1047. doi:10.1007/s00247-006-0264-5

8. Kosciuch J, Przybylowski T, Gorska K, et al. [Relationship between airway basement membrane thickness and lung function tests in patients with asthma]. *PneumonolAlergolPol*. 2009;77(3):256-263.
9. Galbán CJ, Han MK, Boes JL, et al. Computed tomography-based biomarker provides unique signature for diagnosis of COPD phenotypes and disease progression. *Nat Med*. 2012;18(11):1711-1715. doi:10.1038/nm.2971
10. Stewart JI, Criner GJ. The small airways in chronic obstructive pulmonary disease. *Curr Opin Pulm Med*. 2013;19(2):109-115. doi:10.1097/MCP.0b013e32835ceefc
11. Niimi A, Matsumoto H, Amitani R, et al. Airway wall thickness in asthma assessed by computed tomography: Relation to clinical indices. *Am J Respir Crit Care Med*. 2000;162(4 I):1518-1523. doi:10.1164/ajrccm.162.4.9909044
12. Oguma T, Hirai T, Niimi A, et al. Limitations of Airway Dimension Measurement on Images Obtained Using Multi-Detector Row Computed Tomography. *PLoS One*. 2013;8(10). doi:10.1371/journal.pone.0076381
13. Saba OI, Hoffman EA, Reinhardt JM. Maximizing quantitative accuracy of lung airway lumen and wall measures obtained from X-ray CT imaging. *J Appl Physiol*. 2003;95(3):1063-1075. doi:10.1152/japplphysiol.00962.2002
14. Lutey BA, Conradi SH, Atkinson JJ, et al. Accurate measurement of small airways on low-dose thoracic CT scans in smokers. *Chest*.

2013;143(5):1321-1329. doi:10.1378/chest.12-0034

15. Gelb AF, Gobel PH, Fairshter R, Zamel N. Predominant Site of Airway Resistance in Chronic Obstructive Pulmonary Disease. *Chest*. 1981;79(3):273-276. doi:10.1378/chest.79.3.273

16. Cottini M, Lombardi C, Micheletto C. Small airway dysfunction and bronchial asthma control : the state of the art. *Asthma Res Pract*. 2015;1(1):13. doi:10.1186/s40733-015-0013-3

17. D. Pare P, L. Wright J, Churg A. Small airway obstruction in chronic obstructive pulmonary disease. In: Voelkel NF, MacNee W, eds. *Chronic Obstructive Lung Diseases*. 2nd ed. Lewiston, NY: BC Decker; 2008:512.

18. Boyden EA. *Segmental Anatomy of the Lungs: A Study of the Patterns of the Segmental Bronchi and Related Pulmonary Vessels*. Vol 43. Wiley-Blackwell; 1955. doi:10.1002/bjs.18004317729

19. American College of Chest Physicians. *Chest : Official Publication of the American College of Chest Physicians*. The College; 1970.

20. Bhatia R. Diseases of Small Airways of lung. *J Indian Acad Clin Med*. 2001;2:223.

21. Hogg JC, Chu F, Utokaparch S, et al. The nature of small-airway obstruction in chronic obstructive pulmonary disease. *N Engl J Med*. 2004;350(26):2645-2653. doi:10.1056/NEJMoa032158

22. Mead J. The Lung's Quiet Zone. *N Engl J Med*. 1970;282(23):1318-1319. doi:10.1056/NEJM197006042822311

23. McNulty W, Usmani OS. Techniques of assessing small airways dysfunction. *Eur Clin Respir J*. 2014;1:25898-

http://dx.doi.org/10.3402/ecrj.v1.25898. doi:10.3402/ecrj.v1.25898

24. Hogg JC, Macklem PT, Thurlbeck WM. Site and Nature of Airway Obstruction in Chronic Obstructive Lung Disease. *N Engl J Med*. 1968;278(25):1355-1360. doi:10.1056/NEJM196806202782501

25. Zamel N. The Real Quiet Zone of the Lung. *Chest*. 1982;81(6):662. doi:10.1016/S0012-3692(16)57744-7

26. James C. Hogg, M.D., Fanny Chu, B.Sc., Soraya Utokaparch, B.Sc., Ryan Woods, M.Sc., W. Mark Elliott, Ph.D., Liliana Buzatu, M.D., Ruben M. Cherniack, M.D., Robert M. Rogers, M.D., Frank C. Sciurba, M.D., Harvey O. Coxson, Ph.D., and Peter D. Paré MD, Abstract. The Nature of Small-Airway Obstruction in Chronic Obstructive Pulmonary Disease. *N Engl J Med*. 2004;351(21):2159-2169. doi:10.1056/NEJMoa1208410

27. Patel BD, Coxson HO, Pillai SG, et al. Airway wall thickening and emphysema show independent familial aggregation in chronic obstructive pulmonary disease. *Am J Respir Crit Care Med*. 2008;178(5):500-505. doi:10.1164/rccm.200801-059OC

28. Grydeland TB, Thorsen E, Dirksen A, et al. Quantitative CT measures of emphysema and airway wall thickness are related to DLCO. *Respir Med*. 2011;105(3):343-351. doi:10.1016/j.rmed.2010.10.018

29. Dijkstra A, Postma D. Low-dose CT measurements of airway dimensions and emphysema associated with airflow limitation in heavy smokers: a cross sectional study. *Respir ....* 2013;14(1):11. doi:10.1186/1465-9921-14-11

30. Mohamed Hoesein FAA, de Jong PA, Lammers JWJ, et al. Contribution of

CT quantified emphysema, air trapping and airway wall thickness on pulmonary function in male smokers with and without COPD. *COPD J Chronic Obstr Pulm Dis*. 2014;11(5):503-509. doi:10.3109/15412555.2014.933952

31. Lutey BA, Conradi SH, Atkinson JJ, et al. Accurate measurement of small airways on low-dose thoracic CT scans in smokers. *Chest*. 2013;143(5):1321-1329. doi:10.1378/chest.12-0034

32. Mohamed Hoesein FAA, de Jong PA, Lammers J-WJ, et al. Airway wall thickness associated with forced expiratory volume in 1 second decline and development of airflow limitation. *Eur Respir J*. 2015;45(3):644-651. doi:10.1183/09031936.00020714

33. Estépar RSJ, Washko GG, Silverman EK, Reilly JJ, Kikinis R, Westin C-F. Accurate airway wall estimation using phase congruency. *Med Image Comput Comput Assist Interv*. 2006;9:125-134.

34. Kim N, Seo JB, Song KS, Chae EJ, Kang SH. Semi-automatic measurement of the airway dimension by computed tomography using the full-width-half-maximum method: a study on the measurement accuracy according to the CT parameters and size of the airway. *Korean J Radiol*. 2008;9(3):226-235. doi:10.3348/kjr.2008.9.3.226

35. Chae EJ, Kim TB, Cho YS, et al. Airway Measurement for Airway Remodeling Defined by Post-Bronchodilator FEV1/FVC in Asthma: Investigation Using Inspiration-Expiration Computed Tomography. *Allergy, Asthma Immunol Res*. 2011;3(2):111. doi:10.4168/aair.2011.3.2.111

36. Weinheimer O, Achenbach T, Bletz C, Düber C, Kauczor HU, Heusse CP.

About objective 3-D analysis of airway geometry in computerized tomography. *IEEE Trans Med Imaging*. 2008;27:64-74. doi:10.1109/TMI.2007.902798

37. Wiemker R, Van Stevendaal U, Schmitt H, et al. Comparison of correction methods for bronchial lumen and wall thickness measurement using a physical tube array phantom. 2013;8668(November 2015):86684W. doi:10.1117/12.2006236

38. Louizos C, Yáñez J a, Forrest ML, et al. Measuring Small Airways in Transverse CT Images. Correction for Partial Volume Averaging and Airway Tilt. *Acad Radiol*. 2010;17(1):1525-1534. doi:10.1016/j.acra.2010.08.005.

39. Conradi SH, Lutey BA, Atkinson JJ, Wang W, Senior RM, Gierada DS. Measuring Small Airways in Transverse CT Images. Correction for Partial Volume Averaging and Airway Tilt. *Acad Radiol*. 2010;17(12):1525-1534. doi:10.1016/j.acra.2010.08.005

40. Achenbach T, Weinheimer O, Dueber C, Heussel CP. Influence of pixel size on quantification of airway wall thickness in computed tomography. *J Comput Assist Tomogr*. 2009;33(5):725-730. doi:10.1097/RCT.0b013e318190699a

41. Markevich N, Gertner I. Comparison among methods for calculating FWHM. *Nucl Instruments Methods Phys Res Sect A Accel Spectrometers, Detect Assoc Equip*. 1989;283(1):72-77. doi:10.1016/0168-9002(89)91258-8

42. Buzug TM. *Computed Tomography : From Photon Statistics to Modern*

Cone-Beam CT. Springer; 2008.

43. Proakis JG, Manolakis DG. *Digital Signal Processing*. Pearson Prentice Hall; 2007.

44. Heo C, Yang Z, Kim J. SU□E□E□04: Automated Analysis of Quality Assurance Phantom Scan Image in Functional Lung CT Study by Using Simulated CT Imaging Technique. *Med Phys*. 2013;40(6). doi:10.1118/1.4814072

45. Prevrhal S, Fox JC, Shepherd J a., Genant HK. Accuracy of CT-based thickness measurement of thin structures: Modeling of limited spatial resolution in all three dimensions. *Med Phys*. 2003;30(1):1. doi:10.1118/1.1521940

46. Newman DL, Dougherty G, al Obaid A, al Hajrasy H. Limitations of clinical CT in assessing cortical thickness and density. *Phys Med Biol*. 1998;43(3):619-626. doi:10.1088/0031-9155/43/3/013

47. Dougherty G, Newman D. Measurement of thickness and density of thin structures by computed tomography: a simulation study. *Med Phys*. 1999;1341(April 1998):1341-1348. doi:10.1118/1.598629

48. Wildberger JE, Mahnken AH, Flohr T, et al. Spatial domain image filtering in computed tomography: feasibility study in pulmonary embolism. *Eur Radiol*. 2003;13(4):717-723. doi:10.1007/s00330-002-1700-z

49. Ohkubo M, Wada S, Matsumoto T, Nishizawa K. An effective method to verify line and point spread functions measured in computed tomography. *Med Phys*. 2006;33(8):2757. doi:10.1118/1.2214168

50. Achenbach T, Weinheimer O, Biedermann A, et al. MDCT assessment of

airway wall thickness in COPD patients using a new method: correlations with pulmonary function tests. *Eur Radiol*. 2008;18(12):2731-2738. doi:10.1007/s00330-008-1089-4

51. Judy P, Estepar SJ, Hoffman E, Lynch D. SU□FF□I□06: COPDGene Study Quality Assurance Phantom. *Med Phys*. 2009;36(6):2435. doi:10.1118/1.3181125

52. Fujita H, Tsai D-Y, Itoh T, et al. A simple method for determining the modulation transfer function in digital radiography. *IEEE Trans Med Imaging*. 1992;11(1):34-39. doi:10.1109/42.126908

53. Boone JM. Determination of the presampled MTF in computed tomography. *Med Phys*. 2001;28(3):356. doi:10.1118/1.1350438

54. Bilmes J a. A gentle tutorial of the EM algorithm and its application to parameter estimation for Gaussian mixture and hidden Markov models. *Int Comput Sci Inst*. 1998;4(510):126. doi:10.1.1.119.4856

55. Feragen A, Petersen J, Owen M, et al. A hierarchical scheme for geodesic anatomical labeling of airway trees. *MICCAI Proc*. 2012;15(Pt 3):147-155. doi:10.1007/978-3-642-33454-2_19

56. Mohamed Hoesein FAA, de Jong PA, Lammers JWJ, et al. Computed Tomography Structural Lung Changes in Discordant Airflow Limitation. *PLoS One*. 2013;8(6). doi:10.1371/journal.pone.0065177

57. Tschirren J, Huffman E a., McLennan G, Sonka M. Intrathoracic airway trees: Segmentation and airway morphology analysis from low-dose CT scans. *IEEE Trans Med Imaging*. 2005;24(12):1529-1539. doi:10.1109/TMI.2005.857654

58. Reinhardt JM, D'Souza ND, Hoffman E a. Accurate measurement of intrathoracic airways. *IEEE Trans Med Imaging*. 1997;16(6):820-827. doi:10.1109/42.650878

59. King GG, Müller NL, Whittall KP, Xiang QS, Paré PD. An analysis algorithm for measuring airway lumen and wall areas from high-resolution computed tomographic data. *Am J Respir Crit Care Med*. 2000;161(2 I):574-580. doi:10.1164/ajrccm.161.2.9812073

60. Voelkel NF, MacNee W. *Chronic Obstructive Lung Diseases*. 2nd ed. Lewiston, NY: BC Decker; 2008.

61. Hsieh J. Investigation of the slice sensitivity profile for step-and-shoot mode multi-slice computed tomography. *Med Phys*. 2001;28:491-500. doi:10.1118/1.1359247

62. Nakano Y, Wong JC, De Jong PA, et al. The prediction of small airway dimensions using computed tomography. *Am J Respir Crit Care Med*. 2005;171(2):142-146. doi:10.1164/rccm.200407-874OC

63. Yamashiro T, Matsuoka S, Estépar RSJ, et al. Quantitative assessment of bronchial wall attenuation with thin-section CT: An indicator of airflow limitation in chronic obstructive pulmonary disease. *Am J Roentgenol*. 2010;195(2):363-369. doi:10.2214/AJR.09.3653

국 문 초 록

내경이 2~3mm미만인 작은 기도의 치수는 천식 및 만성 폐색종(COPD)과 같은 폐 질병을 평가하기 위한 중요한 생체 지표이나, CT 시스템의 해상도의 한계는 소기도 치수를 결정하는 데 방해요인이 되었다. 본 연구에서는, 작은 기도 치수와 강력한 CT스캔 파라미터를 정확하게 결정할 수 있는 새로운 방법인 감쇠 프로필 매칭 방법을 제공한다.

폐 기도의 감쇠 프로파일을 생성하기 위해, 다양한 벽 두께에 따른 수치 폐 기도 모델을 생성하고, CT시스템에서 획득한 점 확산 기능을 컨볼루션하여 계산하였다. 기도의 치수는 기도의 전체 각도에 걸쳐 측정된 감쇠 프로필과 수치 모델에 의해 합성된 감쇠 프로필 사이의 최소 오차를 산출하는 계산식에 따라 결정되었다.

기도 관 팬텀 연구에서, 제안된 방법은 기도 벽 두께를 결정하는 데 매우 정확하다는 것이 입증되었다. 직경이 3mm인 0.6mm두께의 튜브에서 측정 오류는 벽 두께의 경우 겨우 2.10mm(3.3%)이고, 기도 내부 직경의 경우 0.17 mm(5.6%)였다. 팬텀 연구는 제안된 방법이 벽 두께 측정 시 매우 정확하다는 것을 입증하였다. 0.6mm두께의 가장 작은 튜브에 대한 오류는 0.001mm였다. 시험 임상연구에서, 제안된 방법은 COPD 군에서 1.16±0.23 mm, 정상군에서 0.6 ± 0.18 mm로 두 군집의 구별이 가능했으며, FWHM 방법의 경우 측정치는 각각 1.45 ± 0.32 mm, 1.28 ± 0.30 mm 로 두 군집간의 구별이 어려웠다.

우리가 제안한 감쇠 프로파일 매칭 방법은 현재 CT시스템의 해상도의 한계를 극복하고 COPD 환자에게 작은 기도 치수를 정확하게 측정할 수 있는 잠재력을 갖고 있다.

주요어 : 감쇠 프로필 매칭, COPD, 소기도, 기도 치수, 벽두께 측정, 점 확산 함수

학 번 : 2013-30738

ACKNOWLEDGMENT

모든 것의 시작과 중심, 끝이 되신 하나님 아버지께 먼저 감사드립니다. 모든 것이 주께서 계획하신 바이며, 그 길을 묵묵히 따라가고 있을 수 있음에 행복합니다.

또한, 저의 모든 것의 시작과 중심이고, 여전히 제 인생의 위인이신 아버지 어머니께도 감사를 드립니다. 목마를 때의 오아시스였으며, 나태할 때의 채찍이었으며, 지칠 때의 기댈 곳이었습니다. 사랑합니다.

2008년 겨울부터 연구실에 들어와, 막내인 듯 외부인인 듯 지낸 게 마냥 얼마 전 이야기 같습니다. 서울대학교병원 의생명연구원 별관 3층 구석에 꿔다 놓은 보릿자루 마냥 어색해 하며 앉아있던, 눈이 잔뜩 오던 어느 날이 기억납니다. 날짜를 더듬더듬 세어 보니, 그 기억은 어느 새 10년 전의 기억입니다.

대학원생으로서 이 자리에 앉아있던 기간을 돌이켜 보면, 정말 다양했던 모습이 많이 그려집니다. 나태하게 앉아 하루 종일 모니터만 쳐다보던 기억, 책상 밑 공간에 엎드려 누워 천장을 바라보며 잠들던 기억, 공부의 벽과 현실의 벽에 부딪혀 펑펑 울던 기억, 너무 지쳐 쓰러졌어도, 다음날 또 너무나 당연한 듯 컴퓨터 앞에 앉아 논문을 폈던 기억, 연말 연시에 다들 들떠 있을 때 자연스럽게 연구실에 출근해버리곤 당황해 했던 기억, 회식 후 술에 가득 취해 늑대 무리 마냥 우르르 몰려다니며 덩실거리던 기억.. 하지만 역시 가장 기억에 남는 건, 몇 년을 공들였던 논문을 처음 제출했던 추석의 어느 날이 아닐까 싶습니다. 웹페이지에서 공들인 클릭 수백 번 후, 업로드 완료라는 메시지와 함께 밀려오던 벅찬 마음에 두어 시간 자리에서 울며 일어날 수 없었던 그 시간이.

모든 기억이 모두 보람차다고 할 수는 없지만, 그 모든 순간이 소중하고 행복했습니다. 대학원 시작 시점으로 다시 돌아가라면 솔직히 엄두는

나지 않습니다만, 같은 사람과 같은 시간을 보낼 수 있다면 다시 돌아가도 좋겠다는 생각을 합니다. 적어도 이제 36년 살아온, 아직 1부 막도 채 내리지 않은 인생 중에서는 가장 빛났던 기간이었습니다.

'왜 박사를 Ph.D. 라고 하는가'에 대해서 연구실 사람들과 이야기한 적이 있습니다. 왜 '철학박사' 라는 통칭으로 우리를 명시하는지에 대해서. 고통스러웠지만 행복했던 대학원생 기간에, 고민하고 공부하며 걱정하고 결정하면서 저에게 가장 큰 바뀐 것 하나라면, '내 분야에 대한 줏대' 인 것 같습니다. 내가 알고 있는, 내가 생각하는 것에 대한 자신감, 그 것을 지키고 갈고 닦으며, 그것에 대해 집중하는 것이 나의 삶이 되었습니다. '나' 라는 것에 또 다른 의미를 부여하는 것, 그 의미를 '철학' 이라는 이름 하에 소중히 간직하는 것이 바로 박사의 의미가 아닐까 생각합니다.

지인들에게서 벌써부터 가끔 불리우는 '박사'라는 호칭이 너무나 어색하고, 아직 저에게는 과분하다는 생각만 듭니다. 그러기에 더더욱, 이 호칭에 부끄럽지 않게 살겠다는 각오를 다시 한번 다집니다.

저에게는 철저하게 교수님이었던 김종효 교수님께 무한한 감사를 드립니다. 시작과 끝, 글자 하나 점 하나까지 같이 고민해 주시고, 짙게 연단하셨으며, 끝까지 중심을 지키시고 마지막까지 함께 하셨습니다. 때로는 넓고 깊은 지식에 감탄하며, 때로는 의도를 이해하지 못하고 왜 그러실까 하며 힘들어했어도, 제가 정한 모토인 '오직 신뢰와 순종' 이라는 단 하나의 키워드로 지냈던 대학원생 기간을 헛되이 만들지 않으셨습니다. 처음부터 마지막까지 철저하게 학생으로, 소중하게 지도하여 주신 것에 가장 큰 감사를 드립니다.

더불어, 본 학위논문의 심사기간 동안 진심 어린 격려와 매서운 조언을 주신 교수님들께 감사를 드립니다. 본 연구에서 미처 보지 못했던 부분으로의 시야를 확장하게 해 주신 이원진 교수님, 정량적이고 정확한 임상적 기준을 세워야 한다는 가르침을 주신 임형준 교수님, 전반적으로 미처 모자란 완성도와, 연구자로서의 설명의 중요성에 대해 정확하게 지

적해 주신 홍헬렌 교수님, 단시간에 섬세하게 연구를 분석하시고 더 정확한 가이드를 세워 주신 선배님 이준구 교수님께 다시한번 큰 감사를 드립니다.

우리 소중한 BICL 연구원들에게도 감사를 드립니다. 앞서 연구실을 이끌어 주시고, 다음 갈 길에 대해서도 소중한 조언을 아끼지 않으셨던 이준구 박사님, 저의 연구실 생활의 시작을 함께 해 주시고, 연구자로서의 중심을 잡아주셨던 이상호 박사님, 언제나 젠틀한 모습과 매서운 판단으로 앞서주셨던 박상준 박사님, 제 연구에 깊은 기반을 만들어 주시고 많은 나이차에도 가족 같고 형제같이 대해 주셨던 김창원 박사님, 제가 흔들릴 때마다 다시 똑바로 세워주신 저와 연구실의 정신적 지주 김영우 박사님, 후배지만 언제나 배울 것이 많았던, 선배보다 멋진 능력을 보여준 우리 강한 남자 전민수 박사에게 감사드립니다.

연구실의 사실상 중간지도자의 역할을 톡톡히 하고 있는 너무나 고맙고 믿음직한 창룡이형, 후배라고 하기엔 이미 동기인, 나 때문에 마음고생 많았던 연구실 삼인방 멤버, 고마운 능력자 동생이자 결혼 선배 유부남 형민이, 걱정과 안심을 둘 다 하게 만드는 신기한 능력을 가진, 재능있고 쾌활한 동네주민이자 미래의 센터 철균이, 엄청난 회사 일정과 가정 생활, 수준 있는 학업까지 세 마리 토끼를 다 잡고 있는 병준씨, 속 많이 썩였지만 그래도 같이 졸업하는 졸업 동기 재원이, 잘 보이지 않지만 있는 곳에서 열심히 하리라 믿는 강원이, 연구실에 새로운 믿음직한 줏대인 장우, 얼마 길게 보지 않았지만 믿음 가고 언제나 열심인 도일이.. 모두 소중한 후배들이며, 후배들을 두고 떠나는 연구실이 한편으론 무겁고 한편으로는 믿음직합니다. 졸업 후에도 언제나 끈끈한 유대를 보여주는 윤섭이형과 우람이, 그리고 많은 지나갔던 학우들과 인턴들에게도 감사드립니다.

고려대학교 구로병원에서 외부연구원으로 연구를 진행할 수 있는 새로운 기회를 주신 용환석 교수님, 우옥희 교수님, 홍석주 교수님과 MIDC 소속 연구원들에게도 감사드립니다. 주어진 기회에 실망시켜드리지 않도

록 노력하겠습니다.

자주 뵙지 못하지만 언제나 응원해 주시는 할머니, 외할머니, 친척들, 사촌들, 기도로써 도와주시는 영은교회 고일호 목사님, 정유근 목사님, 언제나 말씀으로 도와주시는 채성애 권사님을 비롯한 많은 은사님들, 친형제보다 더 형제 같은 태화형과 민채 및 페인댄서 형동생들, 공부한답시고 자주 못 본 벌써 20년을 훌쩍 넘은 친구들인 나우누리 신서중학교 통신모임 멤버들, 준영이형, 순영이형, 형훈이형, 철희, 창원이, 성규, 정원이, 정현이, 국민학교 시절부터 같이 비빈 광규, 일규, 이제는 자주 보지 못하는 신정네거리 네버다이 패밀리와 목동아파트 11단지 독서실 가족들, 지치고 힘들 때마다 고마운 휴식처가 되어 준 양원이형 및 일동비엔 가족들.. 지면 상의 이유로 채 이름을 기입하지 못한 다른 모든 분들에게도 감사를 전합니다.

그리고, 앞으로 계속 함께 할 나의 단 한 명, 박민영씨에게도 감사를 전합니다. 이제 모든 것은 당신만을 위해.

앞으로 '난 아직 모자르니까' 라는 말을 변명으로 쓰지 않겠습니다. 저의 주된 원동력으로 삼겠습니다. 한 명의 연구자로서, 매섭게 나와 주변을 살피되 주어진 길을 묵묵히 걸어가는 虎視牛行(호시우행)의 자세로, 또한 오직 하나님의 아들로 걸어갈 것을 다짐하며 감사의 글을 마칩니다.